Title
Elucidating virulence effectors important for M. tuberculosis survival in the host macrophage

Author
Lien, Katie Ann

Publication Date
2018

Peer reviewed|Thesis/dissertation

Elucidating virulence effectors important for *M. tuberculosis* survival in the host macrophage

By

Katie A. Lien

A dissertation submitted in partial satisfaction of the

requirements for the degree of

Doctor of Philosophy

in

Molecular and Cell Biology

in the

Graduate Division

of the

University of California, Berkeley

Committee in charge:

Professor Sarah Stanley, Chair
Professor Daniel Portnoy
Professor Russell Vance
Professor Kathleen Ryan

Fall 2018

Abstract

Elucidating virulence effectors important for *M. tuberculosis* survival in the host macrophage

By

Katie A. Lien

Doctor of Philosophy in Molecular and Cell Biology

University of California, Berkeley

Professor Sarah Stanley, Chair

The host-pathogen interaction during *M. tuberculosis* infection is dynamic and complicated. Many mechanisms of cell intrinsic control are up-regulated in response to *M. tuberculosis* infection. However, *M. tuberculosis* regulates its immediate environment and forms a replicative niche inside phagosomes, the same vesicles in which most pathogens die.

In the introductory chapter of this dissertation, I highlight the major ways in which macrophages, the cell type *M. tuberculosis* predominantly infects, are activated during infection to become inhospitable to invading pathogens. The most important are mechanisms mediated by IFN-γ, a cytokine that regulates an intricate network of pathways. I then address a few ways in which *M. tuberculosis* is able to inhibit or counteract host antimicrobial responses and persist in the phagosome. Specifically, I address the bacteria's ability to survive and mitigate the effects of acid and oxidative stress in the phagolysosome.

In the second chapter, I profile differences between the mouse and human macrophage environment. IFN-γ stimulated human macrophages infected with *M. tuberculosis* up-regulate mechanisms of cell intrinsic control, but are unable to restrict bacterial growth. This is in stark contrast to mouse macrophages that display significant restriction of *M. tuberculosis* growth when activated with IFN-γ. The differences in macrophage environment have physiological consequences for the bacteria. During *M. tuberculosis* infection of human macrophages, bacteria undergo nitrogen metabolism and produce robust amounts of nitrite. During mouse macrophage infection, nitrite detected is produced by the host as a byproduct of IFN-γ activation and production of NO. To indiscriminately identify genes that are essential for survival in the different physiological environments of human and mouse macrophages, I perform a transposon-sequencing screen. Preliminary analysis of this data set reveals

identification of new genes that will be used to spur future research and elucidate mechanisms of survival.

In chapter three, I characterize a bacterial organelle that is essential for *M. tuberculosis* survival under conditions of oxidative and pH stress. The nanocompartment is a proteinaceous organelle that packages a dye-decoloring peroxidase (DypB) inside. Unlike most peroxidases, DypB is optimally active at acidic pH levels and has an essential function in conditions where other enzymes are inactivated. This is in part due to its optimal activity at low pH, but also because the peroxidase is packaged in the protective environment of the nanocompartment shell. Packaging of the dye-decoloring peroxidase inside of the nanocompartment is necessary for maximal survival of *M. tuberculosis* when bacteria are exposed to oxidative and acid stress. Additionally, nanocompartment mutants are attenuated for growth during macrophage infection, proving nanocompartments mediate bacterial survival within the phagolysosome.

I close with a final chapter in which I speculate on the future directions of each project. In particular, I discuss the newer technology of random barcoded transposon sequencing (Bar-seq). Bar-seq will have a tremendous impact on improving the essentiality predictions of *M. tuberculosis* genes as it is better suited for analyzing slow growing bacteria that have smaller magnitudes of separation between attenuated and fully-virulent mutants. Additionally, the simple and cost-effective design of Bar-seq will allow for high-throughput screening of *M. tuberculosis* mutants through hundreds of chemical conditions to improve gene annotation. As for the role of bacterial nanocompartments, one of the looming questions is whether the organelle is stable enough to function extracellularly in a phagolysosome and protect bacteria. Future directions will further characterize the organelle versus organelle battle between host phagolysosomes and bacterial nanocompartments.

Dedication

To my parents, Shannon and Garth
To my grandmothers, Geraldine and Cleone

You are the wells from which I draw

Table of Contents

List of Figures and Tables

Acknowledgements

My first thanks are to Sarah. Not only is she a brilliant scientist, but she truly shines as a mentor, both scientific and otherwise. She shaped my scientific acumen, provided a healthy dose of optimism to counter my pessimism, and reminded me that being a good scientist does not have to be at the expense of being human. To her, I owe a great deal. In addition to my PI, I have been fortunate to have many terrific advisors through out graduate school. Jeff Cox came to Berkeley half way through my grad school career and has such pure excitement for science, which is contagious. The Cox lab has been a great group to have joint lab meetings with and I am especially grateful for the help and scientific advice of Bennett Penn. Bennett served as an endless source of reagents and laughs, and even as a needle-cushion on an occasion or two. The members of my thesis committee, Kathleen Ryan, Russell Vance, and Dan Portnoy have been exceptional in providing guidance throughout graduate school. Dan Portnoy was one of the people who influenced my decision to attend Berkeley and has gone particularly above and beyond with his support.

When I first joined the Stanley lab, it was very small. It has since grown a lot, but it has always been filled with people I have the privilege to call friends in addition to co-workers. They are a wonderfully smart, supportive and sassy group, and because of them grad school has not been measured by the number of experiments. Together we've performed countless hours of BSL3 karaoke, watched more pimple-popping videos than one should, lost so many nerf darts, and probably looked at every dog photo on the internet. Jonathan Braverman, Kim Sogi, Matt Knight, Robyn Jong, Marietta Ravesloot-Chavez, Erik Van Dis, Dan Fines and Ronald Rodriguez have helped me through the days when the sweatshirt hood gets pulled up, and for that I could not be more grateful. In addition to Stanley lab members, I had amazing collaborators in the Savage lab. Rob Nichols and Caleb Cassidy-Amstutz were great colleagues and I loved working on the nanocompartment project with them.

Since coming to graduate school, I have added to the list of people who are permanently stuck with me in their lives. Laura Wetzel, Justin De Leon, Ethan Mc Spadden, Alison Stanbery, Kayley Hake, Erik Van Dis, Matt Knight, and Jonathan Braverman have been there through it all. From their weird senses of humor to their exceptionally big hearts and love for going full-lo at Molo, they have helped me call Berkeley "home." Graduate school would not have been nearly as fun without them.

My most important and difficult to articulate thanks goes to my family. My parents, grandparents, brother, sister-in-law, sweet baby nephews, and best friend, Molly Esteve, are endless with their love, support, and resolute belief in me. They have provided me with everything I need, and then so much more. For my parents in particular, there are no words to adequately describe how their

encouragement and love have influenced me. I could not have done this without them.

While not technically lab members, I must acknowledge a few additional people and things. J.K. Rowling's books have enchanted me with their magic since childhood and helped me through hours of tissue culture work while I was optimizing experiments, much to the dismay of labmates. My Pandora and Spotify accounts provided a very loud soundtrack to many hours of plating for CFU, much to the dismay of the lab next door to the BSL3. My computer was a stalwart companion and survived many falls, late nights of data analysis, afternoons being perched too close to my stove, and successive months of never being properly shut off. It only caused me dismay when it asked to be updated every night. Finally, I must acknowledge the countless others who have come before graduate school and throughout it. These people have fostered my love for science, helped me celebrate the highs, and reminded me that sometimes the snake is just a rope.

Chapter One

Introduction

1.1 Prevalence and significance

It was called 'Pthisis' or 'wasting away' by the Ancient Greeks because the disease looked like it was consuming the infected. In the 18th century, it was called 'The White Plague' due to the sickly and pale complexion of dying patients (Barberis et al., 2017). Today, it is called tuberculosis, named after the etiological bacteria species *Mycobacterium tuberculosis*. Currently, 1.7 billion people are infected and tuberculosis continues to be the leader in mortality caused by a single infectious disease. In 2017 alone, 1.3 million people died from tuberculosis and 10 million people were newly infected (WHO Global Tuberculosis Report, 2018). While tuberculosis is an ancient disease that has persisted in humans over thousands of years, only 10% of those infected with *M. tuberculosis* will develop the active disease and become ill. The duality of being a pathogen that is predominantly sequestered in human hosts in a latent stage and a disease that is so pervasive and exploitative of compromised humans sets the stage for research studying the dynamic interface between host-tuberculosis interactions.

1.2 Establishment of infection

Pulmonary tuberculosis is spread via aerosolization of bacteria from the lungs of individuals infected with the active disease as they cough, speak, and laugh. The aerosolized bacteria are inhaled and subsequently phagocytosed by alveolar macrophages in the lungs of people nearby (Russell, 2006). After initial infection, alveolar macrophages secrete the pro-inflammatory cytokine TNFα and a variety of chemokines, including CXCL10, to recruit neutrophils, monocytes, and lymphocytes to the site of infection (Algood et al., 2003; Russell, 2006). IL12 production from infected macrophages stimulates robust secretion of IFN-γ from $CD4^+$ T cells (Cooper et al., 1997). In turn, IFN-γ simultaneously activates macrophages to become microbicidal and helps down-regulate the cytokine cascade and cease cell infiltration to the lungs (Cooper, 1993; Ehrt et al., 2001). The result of extensive cell migration to infected macrophages before the onset of IFN-γ is the classic granuloma structure found in human lungs. The granuloma is organized with infected macrophages at a hypoxic center. Adjacent to infected macrophages are foamy macrophages filled with lipid droplets and uninfected monocytes, which are surrounded by lymphocytes and a fibrotic cuff (Russell, 2006). The latent stage of tuberculosis infection is characterized by sequestration of *M. tuberculosis* in the granuloma and the infected individual is not contagious, nor do they develop symptoms. Progression to the active form of the disease is often initiated when the patient becomes immunocompromised for a variety of reasons, including co-infection, malnutrition, or old age, at which time the granuloma turns into a necrotic lesion and releases bacteria into the airways.

1.3 IFN-γ dependent mechanisms of bacterial control in macrophages

Transition to the active disease as the patient becomes immunocompromised is correlated with a marked decrease in $CD4^+$ T cell number or function (Havlir and Barners, 1999). As previously stated, $CD4^+$ T cells secrete IFN-γ, which activates infected macrophages to enhance cell-intrinsic control. One of the most studied IFN-γ regulated mechanisms is up-regulation of inducible nitric oxide synthase (iNOS) and NO production (Flynn et al., 1993). Mice deficient in iNOS are almost as susceptible as IFN-γ knockout mice to *M. tuberculosis* infection and display a hyperinflammatory response (Cooper et al.,1993; MacMicking et al., 1997). In addition to having direct antimicrobial properties that kill *M. tuberculosis* (Chan et al., 1992), NO acts as second messenger to orchestrate signaling events leading to bacterial restriction. Work from our lab has shown that NO stabilizes hypoxia inducible factor-1α (HIF-1α), a transcription factor that regulates expression of ~45% of genes associated with IFN-γ activation such as cytokines, chemokines, and eicosanoids (Braverman et al., 2016). Intriguingly, our lab also demonstrated HIF-1α and iNOS exist in positive feedback loop to increase the immune response to *M. tuberculosis* infection (Braverman and Stanley, 2017). The role of iNOS in enhancing the inflammatory response to *M. tuberculosis* initially seems at odds with the fact that iNOS KO mice display a hyperinflammatory phenotype when infected. However, NO signaling has robust anti-inflammatory effects as well. Nitrosylation of the NLRP3 inflammasome by NO results in inhibition and decreased production of the pro-inflammatory cytokine, IL-1 (Mishra et al., 2013). Additionally, or lab has shown iNOS suppresses NF-κB activity, a transcription factor well noted for its regulation of cytokine production (Braverman and Stanley, 2017). Thus IFN-γ, through iNOS and HIF-1α regulation, finely orchestrates a balanced immune response to combat infection.

As key players of the innate immune system, macrophages execute a wide range of antimicrobial effector functions in response to IFN-γ and infection beyond induction of iNOS and NO production. Other possible mechanisms include sequestration of nutrients from the bacteria (Zhang et al., 2013), production of antimicrobial peptides (Alonso et al., 2007), initiation of autophagy, production of reactive oxygen species, enhanced phagolysosome fusion, and activation of a large family of IFN-inducible GTPases that partially regulate the latter three mechanisms listed (MacMicking et al., 2003; Kim et al., 2007; Kim et al., 2012). While research has tried to pinpoint exactly which of these IFN-γ mechanisms is responsible for increased susceptibility of IFN-γ deficient mice in comparison to iNOS knockout mice, there is no obvious single candidate and it is likely a combination of factors.

1.4 M. tuberculosis mechanisms of persistence within the phagosome

Despite the antimicrobial arsenal employed by macrophages to restrict pathogen growth, *M. tuberculosis* can persist within the cell. Exactly how *M. tuberculosis* manages this feat is not well understood. One of the more interesting facets of this phenomenon is that *M. tuberculosis* forms a replicative niche within the phagosome of macrophages. Following phagocytosis of a pathogen, the phagosome matures and fuses with acidified lysosomes to form the phagolysosome complex. Lysosome fusion delivers hydrolytic enzymes that are preferentially active in the acidic environment and facilitate breakdown of proteins, carbohydrates, nucleic acids, and lipids (Xu and Ren, 2015). However, *M. tuberculosis* blocks maturation of the phagolysosome by secreting mycobacterial protein kinase G (PknG), which modulates a host RabGTPase involved with lysosomal fusion (Vandal 2009; Pradhan et al., 2018). Activation of infected macrophages by IFN-γ enhances phagolysosome fusion by increasing targeting of IRGM1 (MacMicking et al., 2003), an IFN-inducible GTPase that binds a special class of lipids, to the phagosome (Tiwari et al., 2009). Loss of IRGM1 results in a marked decrease in lysosome fusion with phagosomes, but a mechanistic explanation for this phenotype lacking. Regardless, after lysosomes fuse with phagosomes, a proportion of *M. tuberculosis* bacteria are still able to maintain a relatively neutral intrabacterial pH and survive the harsh degradative environment (Vandal et al; 2008). Several genes have been identified as essential for conferring protection of *Mycobacterium tuberculosis* to phagolysosome stress. The most characterized gene, Rv3671c, encodes a membrane serine protease that is not only essential for protection against low pH levels, but is preferentially activated by oxidative stress. Rv3671c mutants maintain intrabacterial pH homeostasis in unactivated macrophages but are quickly acidified upon macrophage activation with IFN-γ. Additionally the mutants are hypersusceptible to H_2O_2 and very attenuated in mice (Vandal et al., 2008; Biswas et al., 2010). It is unclear why a membrane serine protease mediates protection to acid stress and is preferentially activated by oxidative stress, but it is hypothesized that it degrades unfolded proteins denatured by the phagolysosome or is otherwise involved with preservation of membrane integrity (Biswas et al., 2010).

Another interesting feature of *M. tuberculosis* that allows it to survive in the phagosome is its limited sensitivity to reactive oxygen species. During infection, *M. tuberculosis* is phagocytosed by macrophages and neutrophils, both of which undergo a respiratory burst to generate reactive oxygen species and kill invading pathogens. Production of ROS is initiated by assembly of NADPH oxidase on the phagosome of infected phagocytes. NADPH oxidase catalyzes the production of superoxide from molecular oxygen. Superoxide is converted to hydrogen peroxide, either spontaneously or by the aid of superoxide dismutases, which is then converted to hypochlorous acid, the reactive agent in bleach, by myeloperoxidases (Bedard and Krause, 2007). Additionally, when

protonated, superoxide forms hydroperoxyl radicals that are extremely reactive with lipids and generate further toxic byproducts. Thus, NADPH oxidase initiates an oxidative assault on pathogens in the phagosome as these molecules destroy proteins, lipids, DNA, and RNA. Mutations in NADPH oxidase in humans results in Chronic Granulomatous Disease, which is characterized by increased susceptibility to fungal and bacterial pathogens, including *M. tuberculosis* (Lee et al., 2008). These data suggest production of ROS is essential for clearance of many pathogens. However, mice lacking functional NADPH oxidase are not more susceptible to *M. tuberculosis* infection. While NADPH mutations result in slightly higher *M. tuberculosis* burden in lungs of mice, this phenotype is transient and resolved at the onset of adaptive immunity when IFN-γ mediated control occurs (Cooper et al., 2000). Protection of *M. tuberculosis* against ROS is mediated by a ROS scavenging glycolipids, such as lipoarabinomannan (Chan et al.,1991; Flynn and Chan, 2001), mycothiol reserves (Newton et al., 2008), and expression of ~15 enzymes that are annotated as a catalase, superoxide dismutases, and peroxidases (Mishra and Imlay, 2012). Additionally, many of the genes identified for bacterial survival during acid stress, like the membrane serine protease previously mentioned, have also been shown to mitigate damage from ROS (Vandal et al., 2009). While the functions of the latter proteins are unknown, the double protection they confer suggests there is a whole subset of protective enzymes that are optimally suited to protect the bacteria in the harsh phagolysosome environment and warrants further study.

1.5 Goals of this study

The host-pathogen interface of *M. tuberculosis* is akin to a molecular game of chess where the identities, let alone functions, of pieces on each side are only marginally understood. As macrophages mount an immunological attack, the bacteria parries, yet we are often left wondering, “But how?” Or, more aptly, we find ourselves writing the phrase “the mechanism remains unclear.” The technical challenges behind working with a slow growing, bio-safety level 3 pathogen that is ill suited to modern techniques has greatly contributed to this issue. However, looming unanswered questions in the present mean exciting answers are in the scientific future. To address some of these questions, I use the broad and indiscriminate approach of transposon-sequencing to profile genes that are essential for survival in host macrophages. I then characterize a bacterial organelle, the nanocompartment, which is exquisitely suited for protecting *M. tuberculosis* against oxidative and acid stress and essential for bacterial survival in the phagolysosome.

Chapter Two

Identification of genes that are essential for survival of *Mycobacterium tuberculosis* in human and mouse host macrophages

2.1 Abstract

Mycobacterium tuberculosis infects macrophages and forms a replicative niche within the phagosome. IFN-γ activation of mouse macrophages up-regulates mechanisms of cell intrinsic control, including expression of inducible nitric oxide synthase (iNOS) and NO, which restricts bacterial growth. In this study we show human macrophages pre-treated with IFN-γ do not up-regulate iNOS or produce NO. Instead, *M. tuberculosis* replicates unencumbered and secretes nitrite. Bacterial production of nitrite is not observed during mouse macrophage infection, which suggests the mouse and human macrophage environment have striking differences that influence bacterial metabolism. While unable to control *M. tuberculosis* infection, we found human macrophages pretreated with IFN-γ do restrict growth of a different intracellular pathogen, *Legionella pneumophila*. Despite differences in control of the two pathogens, RNA-sequencing shows stimulated human macrophages infected with either pathogen similarly up-regulate gene transcripts canonically associated with IFN-γ activation and immune response. To better understand how *M. tuberculosis* survives in the different macrophage environments, we performed a transposon-sequencing (Tn-seq) screen. *M. tuberculosis* transposon mutants were serially passaged through human and mouse macrophages (with and without IFN-γ activation) and genes that are conditionally essential for *M. tuberculosis* survival in macrophages were identified.

2.2 Introduction

Mycobacterium tuberculosis is the causative agent of tuberculosis, which kills more people than any single infectious disease in a given year (WHO Global Tuberculosis Report, 2018). Pulmonary tuberculosis is spread when a person with the active disease aerosolizes bacteria in their lungs by forceful exhalations, such as coughing. Following inhalation by nearby people, bacteria are phagocytosed by alveolar macrophages in the lung. As canonical members of the innate immune system, macrophages play an integral role in pathogen restriction. Upon activation with IFN-γ, infected macrophages up-regulate mechanisms of cell intrinsic control. Such mechanisms include expression of inducible nitric oxide synthase (iNOS) and NO production (MacMicking et al., 1997), sequestration of nutrients (Zhang et al., 2013), MHC II antigen presentation (Harding and Boom, 2010), production of antimicrobial peptides (Alonso et al., 2007), and activation of IFN-inducible GTPases, which regulate phagolysosome fusion, production of reactive oxygen species and other immunological functions (MacMicking et al., 2003; Kim et al., 2007).

Despite the restrictive environment of the macrophage, *Mycobacterium tuberculosis* can persist and form a replicative niche within the phagosome. To understand why, studies have focused on identifying genes that are essential for bacterial survival within model host organisms or different restrictive conditions

(Sassetti and Rubin, 2003; Rengarajan et al., 2005; Griffen et al., 2011; Zhang et al., 2012). In the past decade, transposon site hybridization (TraSH), which used DNA microarrays, was the primary tool for such research. As the result of sequencing technology advancements, a newer procedure, transposon-sequencing (Tn-seq), has allowed for more sensitive and precise analysis of conditionally essential genes. Both TraSH and Tn-seq screens involve creating a library using transposon mutagenesis. For *M. tuberculosis*, a bacteriophage delivers a plasmid coding for a transposon and transposase, which integrates the transposon randomly within the genome. Selective pressures are applied to the transposon mutant library, and surviving bacteria are sequenced. In 2005, a TraSH screen was performed in primary mouse bone marrow-derived macrophages that were untreated, pre-treated, or post-treated with IFN-γ (Rengarajan et al., 2005). Genes identified as essential for survival in mouse macrophages included ones involved in fatty acid metabolism, components of the type VII secretion system (ESX-1), and small molecule transporters for sugars and inorganic phosphates. While very informative, a study by Griffien at al. demonstrated the enhanced capability of Tn-seq to classify conditionally essential genes, accurately map transposon sites, and ultimately reduce the number of false positives identified during a screen (2011). To date, TraSH or Tn-seq screens have been performed in broth and mice, but only a TraSH screen has been performed in primary mouse macrophages.

While mice are insightful and useful tools for understanding immunological responses to *Mycobacterium tuberculosis*, there are some discrepancies between mice and humans. As an ancient disease, humans and *M. tuberculosis* have co-evolved. Humans are simultaneously resistant to infection and the sole natural reservoir. In the event active disease does occur, activation timing and symptom presentation vary (Menzies et al., 2018; Behr et al., 2018) and are tracked with certain environmental and genetic corollaries (Laurent et al., 2013; Smith et al., 2016). Still, a hallmark of human infection is granuloma formation in lungs. Infected macrophages and foamy macrophages are surrounded by lymphocytes and a fibrotic cuff that are formed as a result of successive cytokine secretion and cellular recruitment. In contrast, there is limited genetic diversity in mouse models, and the standard mouse strain (C57BL/6) does not develop granulomas. Research has focused on correcting these two limitations, and a mouse strain that develops granuloma-like lesions has been identified (Kramnik and Beamer, 2016; Smith et al., 2016). Still, disease outcome during mouse infection does not model human infection as all mice eventually succumb to the disease (Modlin and Bloom, 2013). An additional difference between mouse and human-derived macrophages (HDMs) is expression of iNOS and NO production. In mouse macrophages, treatment with IFN-γ and TLR stimulation up-regulates iNOS expression (Bogdan, 2001; Braverman and Stanley, 2017). In contrast, there is on-going controversy as to whether human macrophages express iNOS (Weinberg, 1998; Schneemann and Schoedon, 2002; Mestas and Hughes, 2004) and some have suggested nitrite detected during *M. tuberculosis*

infection of human macrophages comes from the bacteria rather than the host (Cunningham-Bussel et al., 2013).

In this study we characterize *Mycobacterium tuberculosis* infection of human macrophages. We confirm that *M. tuberculosis* can infect human macrophages and replicate with limited restriction, even when cells are pretreated with IFN-γ and vitamin D. In the human macrophage environment, we show bacteria have altered nitrogen metabolism and produce nitrite, which does not occur in mouse macrophages. Additionally, we find that while IFN-γ pretreatment of human macrophages does not inhibit *M. tuberculosis* growth, the macrophages are activated and up-regulate mechanisms of cell intrinsic control. These findings establish there are remarkable differences between human and mouse macrophages that certainly impact *M. tuberculosis* and provide the rationale for performing a transposon-sequencing screen in cell types from both species.

2.3 Materials and Methods

2.3.1 Ethics statement

All procedures involving the use of mice were approved by the University of California, Berkeley Institutional Animal Care and Use Committee (protocol no. R353-1113B). All protocols conform to federal regulations, the National Research Council's *Guide for the Care and Use of Laboratory Animals*, and the Public Health Service's *Policy on Humane Care and Use of Laboratory Animals*. All human samples were de-identified and approval from the Institutional Review Board was not required.

2.3.2 Reagents

Human rIFN-γ (CAA31639), human rGM-CSF (215-GM-010), and mouse rIFN-γ (5-MI-100) were obtained from R&D System and were used at specified concentrations. Histopaque Ficoll (H8889) and Nω-Nitro-L-arginine methyl ester hydrochloride (L-NAME) were obtained from Sigma Aldrich and L-NAME was used at 100 μM concentrations. 1α,25-Dihydroxyvitamin D3 (vitamin D) was obtained from Enzo Life Sciences and used at 100 nM concentrations. MACS human $CD14^+$ MicroBeads (130-050-201) were obtained from Miltenyi Biotec.

2.3.3 Mouse cell culture

Macrophages were derived from bone marrow of C57BL/6 mice by flushing cells from femurs and culturing in DMEM with 10% FBS and 10% supernatant from 3T3-M-CSF cells for 6 days, with feeding on day 3. After differentiation, BMDMs continued to be cultured in BMDM media containing M-CSF. Cells were cultured at 20% O_2 except infections used for griess assays where MBMDMs were cultured at 10% O_2 to match HDM culture conditions.

2.3.4 Human cell culture

Buffy coat from whole blood (30 mL) was obtained from the Stanford Blood Center. Monocytes were isolated from peripheral blood mononuclear cells by Histopaque Ficoll centrifugation followed by immunogenic labeling with MACS human CD14 MicroBeads. In brief, buffy coats were brought to a final volume of 60 mL with PBS and divided into two batches. Each batch was gently layered over 20 mL of Ficoll and centrifuged at 750 x g for 20 minutes with no brake applied. Following centrifugation, the top plasma layer was aspirated and the middle peripheral blood mononuclear (PBMC) layer was collected. PBMCs were washed in 50 mL of PBS three times with centrifugation at 350 x g for 10 minutes in between wash steps. Following washing, $CD14^+$ monocytes were separated with MACS CD14 MicroBeads according to the manufacturer's instructions. Following separation, cells were re-suspended in RPMI-1640 containing 1X non-essential amino acids, 1X Na-Pyruvate, 2mM GlutaMAX, 10 ng/mL rGM-CSF and 40% male AB human serum. Cells were plated at a density of 3e5 cells and 1.5e6 cells per well in 96 and 24-well poly-d-lysine coated plates, respectively. Following 1 hour of incubation, non-adherent cells were removed and fresh media was replaced. Cells were differentiated for at 20% O_2 14 days with 40% media changes performed every other day. Following infection, rGM-CSF was removed from the media and cells were cultured at 10% O_2.

2.3.5 Mycobacterium tuberculosis bacterial strains and plasmids

The *M. tuberculosis* strain H37Rv was used for all experiments except infections performed for luminescent growth curves and Griess assays, where Erdman strain was used. The luminescent strain is an Erdman-derived strain expressing codon-optimized luxBCADE (Craney et al., 2007). The transposon mutant library was generated in H37Rv.

2.3.6 M. tuberculosis bacterial cell culture

For infections, *M. tuberculosis* was grown to mid-log phase (OD_{600} nm 0.5-1.0) in Middlebrook 7H9 liquid media supplemented with 10% albumin-dextrose-saline, 0.4% glycerol, and 0.05% Tween-80 or on solid 7H10 agar plates supplemented with Middlebrook OADC (BD Biosciences) and 0.4% glycerol. 7H10 plates were supplemented with Kanamycin (50 µg/mL) and 0.05% Tween-80 for growth of transposon mutants.

2.3.7 Legionella pneumophila bacterial cell culture

For infection, a luminescent version of the *L. pneumophila* strain LP02 ΔflaA was used. It is a streptomycin-resistant thymidine auxotroph derived from LP01 and a gift from R. Vance. Bacteria were streaked from glycerol stocks onto BYCE

agar supplemented with streptomycin (100 µg/mL) and grown for 3 days. A single colony was patched onto BYCE agar and grown for 2 days. The patch was re-suspended in BYCE broth supplemented with L-cysteine (0.4 g/L), ferric nitrate (0.135 g/L) and thymidine (0.100 g/L) and grown overnight. Infections were performed using bacteria with OD_{600} nm 3.5-4.5.

2.3.8 M. tuberculosis in vitro infections

HDMs or BMDMs were plated onto 24 or 96-well dishes. HDMs were seeded at a density of 1.5e6 and 3e5 cells per well, respectively. BMDMs were seeded at a density of 2.5e5 and 5e4 cells per well, respectively. Following plating, BMDMs were allowed to adhere overnight, and HDMs were allowed to adhere throughout the 2-week differentiation prior to infection. For all experiments where pre-treatment of cells occurred (IFN-γ, vitamin D, L-NAME), cells were allowed to rest for 24 hours prior to treatment and treated for 24 hours prior to infection. Cells were pre-treated with IFN-γ (5 ng/mL, unless specified), vitamin D (100 nM), and L-NAME (100 µM) and then infected with DMEM supplemented with 5% FBS and 5% horse serum (BMDMs) or RPMI supplemented with 10% male AB serum (HDMs) at the multiplicities of infections specified. Following a 4-hour phagocytosis period, infection media was removed and cells were washed with room temperature PBS before fresh, complete media was added. Cells that had been pre-treated prior to infection had the respective reagents added back to the media following the 4-hour phagocytosis. For CFU enumeration, media was removed and cells were lysed in water with 0.5% Triton-X and incubated at 37°C for 10 minutes. Following the incubation, lysed cells were re-suspended and diluted serially in PBS with 0.05% Tween-80. Dilutions were plated on 7H10 plates. Bacterial luminesce was measured at specified time points using a Spectromax L (Molecular Dynamics).

2.3.9 L. pneumophila in vitro infections

HDMs were plated onto 24 or 96-well dishes. HDMs were seeded at a density of 1.5e6 and 3e5 cells per well, respectively. HDMs were allowed to adhere throughout the 2-week differentiation prior to infection. For all experiments where pre-treatment of cells occurred (IFN-γ, vitamin D), cells were allowed to rest for 24 hours prior to treatment and treated for 24 hours prior to infection. Cells were pre-treated with IFN-γ (5 ng/mL, unless specified), vitamin D (100 nM) and then infected with RPMI supplemented with 10% male AB serum (HDMs) at the multiplicities of infections specified. Spin infections were performed by centrifuging plates at 1200 RPM for 10 minutes at room temperature. Cells were incubated for 1 hour at 37°C before infection media was removed and replaced with standard media supplemented with thymidine. *L. pneumophila* infections performed for RNA-seq did not have thymidine added to the media. Bacterial luminesce was measured at specified time points using a Spectromax L (Molecular Dynamics).

2.3.10 Griess assays

The Griess reaction was used to detect nitrite in the supernatants of HDMs or MBMDMs. In brief, 0.2% napthylethylenediamine dihydrochloride was mixed 1:1 with solution containing 2% sulfanilamide and 4% phosphoric acid to make Griess reagent. Supernatant from cultured cells was added to equal amounts of Griess reagent and absorbance was measured at 546 nm. Concentrations were calculated by comparing absorbance readings to a nitrite standard curve generated in the appropriate cell culture media.

2.3.11 RNA-seq

HDMs were seeded in 24-well plates at a density of 1.5e6 cells per well and infected as described. For RNA-seq, three independent experiments were performed. At 24 hours post-infection, cells were washed with room temperature PBS and lysed in 500 μL of TRIzol (Invitrogen Life Technologies, Carlsbad, CA, USA). Total RNA was extracted using chloroform (100 μL), and the aqueous layer was further purified using RNeasy spin columns (Qiagen, Limburg, Germany). For each sample in each experiment, two duplicate wells were pooled. RNA-seq was performed at the Genome Center and Bioinformatics Core Facility at the University of California—Davis (Davis, CA, USA). SR50 reads were run on an Illumina HiSeq3000, with ~30 million reads per sample. Data analysis was performed by the University of California—Davis bioinformatics group using FastQC for read quality assessment, Sythe and Sickle for Illumina adapter and quality trimming, and Tophat2 for read alignment. Raw counts were derived from alignments using a STSeq-count python script. Tests of differential expression were conducted using a multifactorial model in edgeR/limma (voom).

2.3.12 Creation of transposon mutant library

The transposon mutants were generated in H37Rv M. tuberculosis using the ΦMycoMarT7 transposon donor plasmid. ΦMycoMarT7 was a gift from M. Shiloh. Transduction of *M. tuberculosis* with phage was performed by following the protocol outlined by Long et al. (2015).

2.3.13 Transposon-sequencing screen in macrophages

Macrophages were differentiated and pre-treated as previously described. HDMs and MBMDMs were seeded at a cell density of 1.5e6 cells per well in 24 well and 6 well dishes, respectively. For each condition, 4 wells were infected as previously described and pooled together at the end of the selection. Cells were infected with a thawed aliquot of the transposon mutant library at multiplicity of infection of 0.25 (1 bacteria per 4 macrophages), and 180,000 mutants were plated on 7H10 agar to serve as the control. The infection was allowed to

proceed for 4 days, at the end of which culture media was not removed. Instead, water with 1.5% Triton-X was added the media of cells for a final concentration of 0.5% Triton-X. Cells were lysed for 10 minutes (MBMDMs) or 20 minutes (HDMs) at 37°C. Following lysis, a portion of the lysate was diluted in PBS with 0.05% Tween-80 bacterial concentration was approximately 15,000/mL. For each condition, diluted bacteria were plated on six 245mm x 245mm 7H10 plates with ~30-40 thousand bacteria per plate. Following 21 days of incubation, bacterial colonies were scraped as outlined below. After pooling and re-suspending the bacteria, a portion was used to re-infect HDMs and MBMDMs and a portion was harvested for genomic DNA. *M. tuberculosis* transposon mutants were serially passaged through macrophages three times and the screen was performed in triplicate.

2.3.14 Genomic DNA isolation from M. tuberculosis transposon mutants

Colonies from each conditions were scraped from six 245mm x 245 mm 7H10 plates into 7H9 media. Bacteria were repeatedly pipetted up and down to de-clump bacteria as much as possible. OD_{600} nm measurements were taken to determine the amount of lysing reagents required. The following volumes listed are per 3e9 bacteria. Bacteria were pelleted by centrifugation and supernatants were removed. Bacterial pellets were re-suspended in 450 uL of re-suspension buffer (25 mM Tris-HCl pH 7.9, 10 mM EDTA, 50 mM glucose) and 50 uL of lysozyme (10 mg/mL in re-suspension buffer) were added. Bacteria were mixed by gentle inversion and incubated at 37°C overnight. Following incubation, 100 µL of 10% SDS and 50 µL of proteinase K (10 mg/mL in water) were added to each sample. Samples were mixed by gentle inversion following the addition of each reagent. Samples were incubated at 55°C for 30 minutes. Next, 200 µL of NaCl (5M) and 160 µL pre-warmed CTAB saline were added and samples were gently mixed between each addition. Samples were incubated at 65°C for 10 min. Equal volumes (1 mL) of chloroform:isoamyl alcohol (24:1) were added and samples were mixed by gentle inversion. Samples were centrifuged at 18,500 x g for 10 min and the top 900 µL of aqueous layer were transferred to new tubes for re-extraction with chloroform:isoamyl alcohol (24:1). Samples were centrifuged as before and the top 800 µL of aqueous layer were moved to a new tube. To 800 µL of aqueous layer, 560 µL of isopropanol was added and samples were mixed by gentle inversion to precipitate DNA and centrifuged as before. The supernatant was aspirated and the DNA pellet was washed with 70% ethanol and centrifuged at 18,500 x g for 5 minutes. The supernatant was aspirated and the DNA pellets were air-dried. DNA pellets were covered in 100 µL of water and stored overnight at 4°C to allow the pellet to dissolve.

2.3.15 Transposon mutant sample preparation and Illumina sequencing

Samples were prepared by the University of California, Davis Genome Center DNA Technologies Core by following the protocol outlined by Long et al. (2015)

from steps included in “Random Shearing of Genomic DNA and End Repair” through “Amplification of Transposon-Chromosomal Junctions.” PE100 reads were run on an Illumina HiSeq with ~20 million reads per sample. Sample alignment and TRANSIT pre-processing were performed by the University of California, Davis Bioinformatics Group as outlined by DeJesus et al. (2015).

2.3.16 TRANSIT Analysis of conditionally essential genes

TRANSIT analysis was performed as specified by DeJesus et al. (2015). Resampling analysis was preformed using the reference genome H37RvBD_prot and the following parameters: for global options, 0% of the N- and C- terminus were ignored; for resampling options, 10,000 samples were taken and normalized using the betageometric function. Correction for genome positional bias was preformed. Statistical significance was determined by p value ≤ 0.05 and log2 fold change ≤-1 or by p-adjusted value ≤ 0.05.

2.4 Results

2.4.1. M. tuberculosis replicates in human macrophages independent of IFN-γ and vitamin D activation

It is well documented that *M. tuberculosis* growth is partially restricted in un-activated mouse bone marrow-derived macrophages. To determine if the same was true of human macrophages, we measured *M. tuberculosis* growth during infection. Human monocytes pooled from four donors were differentiated into macrophages (HDMs) and infected with *M. tuberculosis*. Over four days of infection, the bacteria grew 6-fold in human macrophages (Fig. 1A) and 3-fold in mouse bone marrow-derived macrophages (MBMDMs) (Fig. 1B). We next tested whether HDMs are activated by IFN-γ to enhance cell intrinsic control of *M. tuberculosis*. To test this, HDMs were pre-treated with IFN-γ 24 hours prior to infection. Interestingly, IFN-γ activation did not restrict bacterial growth in human macrophages (Fig. 1A), whereas mouse BMDMs activated with IFN-γ significantly inhibited *M. tuberculosis* growth (Fig. 1B). Previous studies have suggested that vitamin D is required for IFN-γ mediated control of *M. tuberculosis* in HDMs as vitamin D enhances production of the antimicrobial peptide cathelicidin (Liu et al., 2006). However, pretreatment of HDMs with IFN-γ and vitamin D had no impact on bacterial growth (Fig. 1A).

2.4.2 Nitrite detected during human macrophage infection is generated by M. tuberculosis

Hallmarks of IFN-γ activated and infected mouse BMDMs are iNOS up-regulation and NO production (Chan et al., 1992). Even though IFN-γ treatment of HDMs did not restrict *M. tuberculosis* growth, we wanted to test if the macrophages were making NO. Whereas IFN-γ pretreatment alone of uninfected

mouse BMDMs, or *M. tuberculosis* infection alone results in weak production of NO (Braverman and Stanley, 2017), IFN-γ and TLR stimulation results in robust NO production within 24 hours, as detected by Griess assays (Fig. 2A). It is important to note that Griess assays detect nitrite (NO_2^-) as a proxy for estimating NO levels. Surprisingly, Griess assays performed on supernatants from resting human macrophages infected with *M. tuberculosis* detected NO_2^- (Fig. 2B, C). Pretreating HDMs with IFN-γ slightly increased the amount of NO_2^- detected in some instances (Fig. 2D), but a dose response with IFN-γ showed that this effect was variable and largely negligible (Fig. 2B). However, increasing the multiplicity of infection of human macrophages did drastically increase values by 24 hours, thus showing the amount of NO_2^- in supernatants correlated to bacterial number (Fig. 2C). A study from Cunningham-Bussel et al. reported that NO_2^- detected in human macrophages infected with *M. tuberculosis* is a byproduct of bacterial nitrogen metabolism (2013). In this scenario, NO is oxidized to nitrate (NO_3^-), which *M. tuberculosis* converts to NO_2^- via the narGHJI nitrate reductase complex. Indeed, NO_2^- levels were significantly decreased in human macrophages infected with ΔnarG mutants, independent of IFN-γ activation, although some was still detected (Fig. 2D). To determine if the residual amount of NO_2^- detected in human macrophages infected with ΔnarG mutant *M. tuberculosis* was originating from bacteria or host cells, HDMs were treated with N omega-nitro-L-arginine methyl ester (L-NAME), an iNOS inhibitor. Treatment with L-NAME did not reduce nitrite production in HDMs infected with wild type or ΔnarG mutant *M. tuberculosis*, suggesting there is a portion of NO_2^- generated by bacteria that is not dependent on the narGHJI nitrate reductase (Fig. 2E). In addition, uninfected HDMs or HDMs infected with heat-killed bacteria had nearly undetectable amounts of NO_2^- (Fig. 2F). These data suggest there are major differences between human and mouse macrophage environments that impact *M. tuberculosis* metabolism. However, we have not ruled out differences that may be attributable to the origin of monocytes from each species (i.e. mouse bone marrow-derived macrophages versus human peripheral blood mononuclear cell-derived macrophages).

2.4.3 Human macrophages are activated by IFN-γ but do not control Mycobacterium tuberculosis infection

While human macrophages did not produce NO in response IFN-γ pretreatment and *M. tuberculosis* infection, we sought to determine if the macrophages were still activated to become microbicidal in other ways. To address this, we infected HDMs with *Legionella pneumophila*, a facultative intracellular pathogen. Previous studies have shown that IFN-γ activation of mouse BMDMs results in significant restriction of *L. pneumophila* bacterial growth (Salins et al., 2001). Similarly, HDMs pretreated with IFN-γ and vitamin D resulted in 6-fold attenuation of *L. pneumophila* growth in 48 hours (Fig. 3A). Despite this, even less NO_2^- was detected in the supernatant of HDMs infected with *L. pneumophila* than with *M. tuberculosis,* again establishing NO_2^- production does

not correlate with bacterial control (Fig. 3B). Since IFN-γ activation of HDMs was sufficient to restrict growth of *L. pneumophila* but not *M. tuberculosis*, we sought to determine if host genes were differentially regulated during infections. To do this, we performed RNA-sequencing on human macrophages infected with either bacteria, with and without IFN-γ and vitamin D pretreatment. After 24 hours of infection, approximately 87% of genes that were ≥8-fold up-regulated by *M. tuberculosis* infection and IFN-γ/vitamin D stimulation were also up-regulated in pretreated cells infected with *L. pneumophila* (Fig. 4A). Approximately 42% of the genes ≥8-fold down-regulated by *M. tuberculosis* infection and IFN-γ/vitamin D stimulation were similarly down-regulated during *L. pneumophila* infection (Fig. 4A). Among the transcripts that were up-regulated in both conditions were IFN-γ-regulated genes involved with MHCII antigen presentation (CIITA), nutrient restriction (IDO1), and the large family of IFN-inducible GTPases (GBP1-7) that help regulate autophagy, initiate assembly of the NADPH phagosome oxidase, and activate the inflammasome (Fig. 4B). However, iNOS was undetectable in all conditions (data not shown). In addition, both bacterial infections with IFN-γ/vitamin D pretreatment up-regulated pro-inflammatory cytokines. Although, transcripts for cytokines including IL12A, TNF, IL10, CXCL1, and CXCL3 were significantly more up-regulated during *L. pneumophila* infection in comparison to *M. tuberculosis* (Fig. 4C). Examination of vitamin D regulated pathways showed that IFN-γ/vitamin D treated macrophages infected with either bacterial species up-regulated the vitamin D receptor (VDR) and an enzyme that converts vitamin D from the inactive pro-vitamin to the active form (CYP27B1). However, while cathelicidin was detectable, it was not up-regulated during infection of IFN-γ/vitamin D activated macrophages (4D).

To predict pathways that were regulated during each infection, we used Ingenuity Pathway Analysis, which assembles experimental datasets into a conglomerate database used to analyze transcriptome data (Fig. 4E). A summary of activation z-score predictions for pathways that are regulated during infection is listed in Table 1, and pathways are sorted by degree of differential regulation. Some of the pathways with the largest differential regulation were TGFβ signaling, Nrf2 mediated oxidative stress response, 14-3-3- signaling, and a variety of cell cycle pathways (all were down-regulated or had lower activation during *M. tuberculosis* infection) (Table 1). However, the most strongly regulated pathways, such as production of NO and ROS in macrophages, TLR signaling, TNF signaling and many other immune response pathways were similarly activated during both infections (Table 1). These data suggest that IFN-γ pretreatment of HDMs is sufficient to activate the macrophages and up-regulate mechanisms of cell intrinsic control. However, either the degree of activation is insufficient to restrict *M. tuberculosis* growth or *M. tuberculosis* is able to regulate the environment and persist in a microbicidal cell. The exact mechanisms by which *M. tuberculosis* survives in an activated human macrophage remain unclear.

2.4.4 Generation of a transposon mutant library in M. tuberculosis

To elucidate mechanisms that allow for *M. tuberculosis* survival in macrophages, we performed a transposon-sequencing screen. To do so, we created a transposon mutant library in H37Rv *M. tuberculosis*. The Himar1 transposon used to create the library is inserted at TA dinucleotide target sequences randomly throughout the genome. Characterization of the mutant library revealed we had 39,491 unique transposon mutants for an insertion density of 54%. The Gumbel method of analysis in TRANSIT, a pipeline used to analyze Tn-seq screen results, can identify genes that are essential in a single condition and is used to evaluate the integrity of a mutant library (DeJesus et al., 2015). Essential and non-essential genes are determined by the number and length of transposon gaps for a given region. With any transposon library, there are regions that lack transposon insertion sites by chance and not because mutation of the gene is lethal. Gumbel analysis can predict the probability of a region void of transposons occurring by chance, and uses those predictions to determine gene essentiality. As summarized in Table 2, approximately 14.5% of genes in H37Rv were essential for survival and 71% of genes were classified as non-essential. Only a small fraction of genes did not have essentiality predictions. Approximately 6.5% of genes were too short to accurately predict essentiality, and 8% of the genes were classified as uncertain if the data were too sparse or if there was essentiality in one domain, but not the entire gene. The classification of genes in our library closely resembled classification of *M. tuberculosis* libraries generated by different labs for Tn-seq studies.

2.4.5 Conditions for performing the transposon-sequencing screen

To perform the Tn-seq screen, human $CD14^+$ monocytes were isolated from buffy coats of four donors and pooled to reduce effects of donor variability. Monocytes were differentiated into macrophages for two weeks using rGM-CSF. Murine bone marrow-derived macrophages were collected by flushing femurs and cells were differentiated for 6 days using supernatant from 3T3-M-CSF cells. Following differentiation, macrophages were pre-treated with IFN-γ (and vitamin D for HDMs) for 24 hours prior to infection, or left untreated. To reduce the risk of macrophages being infected by more than one mutant, cells were infected at a multiplicity of infection of 1 bacteria per 4 macrophages. The infection proceeded for four days, at the end of which macrophages were lysed and the surviving bacterial mutants were plated on 7H10 agar. Surviving mutants grew for 21 days, and the colonies were collected. A portion of the bacteria were harvested for genomic DNA and sequencing, and another portion was used to for additional round of selections (Figure 5). Macrophage screens always have a bottle-neck and since *M. tuberculosis* is a very slow-growing pathogen, we were concerned that there would be insufficient growth to discern which mutants were attenuated for survival. To mitigate this, mutants were

sequentially passaged through macrophages three times, and the screen was performed in triplicate.

2.4.6 Classification of conditionally essential genes

Results from each round of selection were analyzed using a pipeline from TRANSIT software designed to perform comparative analyses (DeJesus et al., 2015). Each experimental condition was compared to the control library that was serially passaged on plates to match the number of selection rounds in macrophages. For a given gene, TRANSIT analysis compares the total number of transposon insertions identified by Illumina sequencing between control and experimental conditions and the fold change and p value are calculated. The analysis also performs a variation of a permutation test to determine the false discovery rate for a given gene, so results can be further refined by a statistically significant p-adjusted value (padj) of ≤ 0.05. For each dataset, we generated two essential gene lists. The first list defined genes as essential by a padj value ≤ 0.05 cutoffs. The second list defined genes as essential if they had a p value ≤ 0.05 and a log2 fold change ≤-1.0. While not surprising, the number of essential genes identified by padj values was staggeringly small in comparison to genes identified by p value and fold change (Table 3). Regardless of the statistical parameters used to classify essentiality, the number of statistically significant hits increased after each passage through macrophages, suggesting multiple rounds of selection in macrophages was beneficial (Table 3). This was further demonstrated when we examined the degree of attenuation for many given mutants after each round of selection. For example, Rv2243, a gene that encodes a malonyl CoA-acyl carrier protein transacylase, was not classified as essential for survival in human macrophages after the first selection as it had a log2 fold change of -0.74 and large padj and p values. However, after multiple rounds of selection, all three statistical parameters used to classify essentiality improved immensely (Table 4), and the gene was identified as conditionally essential (log2 FC= -5.4; p val = 0.0015).

2.4.7 Tn-seq screen identifies M. tuberculosis genes that are essential for survival in macrophage cells

For downstream analysis, we used the list that defined genes as essential by p value and log2 fold change cutoffs. The list was further refined by removing genes that were required for survival of *M. tuberculosis* and result in lethality when mutated (as identified in Table 2), but made it on to the list with very low transposon insertion numbers. A summary of the results for conditionally essential genes identified after three passages through macrophages can be found in Figure 6. In brief, 219 and 183 genes were identified as essential for survival in human macrophages and human macrophages activated with IFN-γ, respectively; 170 and 163 genes were identified as being essential for survival in mouse macrophages and mouse macrophages activated with IFN-γ,

respectively. Of those genes, 38 were considered essential for survival of *M. tuberculosis* in both macrophage types, independent of activation status (Fig. 4, Table 5).

The TraSH screen in mouse macrophages performed by Rengarajan et al. (2005) identified 111 genes as being essential for growth in mouse macrophages (with or without IFN-γ treatment). The statistical parameters used to classify essentiality in the TraSH screen (p value ≤ 0.05; log2 FC ≤ -1.3) varied slightly from ours (p value ≤ 0.05; log2 FC ≤ -1.0). We re-analyzed our data using the same fold change cutoffs and compared the datasets. Our Tn-seq screen identified 376 genes as being essential for growth in any macrophage type (with or without IFN-γ treatment), with 51 genes being identified in both screens (Fig. 7). The larger number of hits identified in our screen partially resulted from the two additional experimental conditions tested (human macrophages +/- IFN-γ). We also compared the hits identified only in mouse macrophages to the TraSH screen: our Tn-seq screen identified 199 genes, with 45 genes overlapping between the two datasets (Fig. 7). This means nearly half (~41%) of the TraSH mutants were identified in our screen, whereas only 23% of hits from our mouse Tn-seq screen were previously identified. All together, the preliminary analyses of our Tn-seq data set suggest we curated a quality list of genes essential for *M. tuberculosis* survival in human and mouse macrophage cells and highlight the enhanced sensitivity of Tn-seq technology.

2.4.8 Preliminary observations of the Tn-seq data set

While serially passaging transposon mutants through macrophages three times did increase the number of hits and improve the dynamic range of our screen, using strict statistical cutoffs to classify conditionally essential genes during analysis still had limitations. Genes were classified as non-essential if either the p value or fold change values did not meet set criteria. In large datasets, there are always hits that are on the cusp of being significant. For example, Rv3541c, a gene encoding a hypothetical protein, was identified as essential for survival in every macrophage condition except mouse macrophages activated with IFN-γ (Table 6). However, without validation, we would be remiss to claim that this gene is not essential for survival in MBMDMs activated with IFN-γ, especially when the raw data revealed the mutant was attenuated, but the p value was slightly too high (p value = 0.0572). This is further exemplified by examination of a gene with known function and importance. Rv3868 encodes a component of the Type VII secretion system, ESX-1, in *M. tuberculosis* (Luthra et al., 2008). Previous studies have shown Rv3868 mutants are attenuated in macrophages (Sassetti and Rubin, 2003; Rengarajan et al., 2005). Despite this, our dataset identified Rv3868 as essential for survival in untreated human and mouse macrophages, but not essential for survival when cells were activated with IFN-γ. Examination of the statistical parameters used to define essentiality revealed that Rv3868 mutants were significantly attenuated in every condition by p value,

but the degree of attenuation as calculated by log2 fold change ratios were not sufficient in macrophages treated with IFN-γ (Table 6).

Still, cutoffs must be applied and the accuracy of predictions is likely to increase as one moves further away from the minimum values required for essentiality. For example, Rv1411c encodes a lipoprotein involved with transporting triacyl glycerides and maintenance of the bacterial cell wall (Drage et al., 2010). To date, Rv1411c is one of the most attenuated mutants found in macrophages (Sassetti and Rubin, 2003; Bigi et al., 2004; Rengarajan et al., 2005). Indeed, analysis of our dataset revealed Rv1411c is unequivocally essential for survival in every macrophage environment (Table 6). Thus, priority for validation will be given to new mutants identified in our screen that are far removed from the statistical cutoff.

2.5 Discussion

In this study, we characterized human macrophage responses to *M. tuberculosis* infection. We found that *M. tuberculosis* grows similarly in unactivated human and mouse macrophages. However, there were striking differences in bacterial growth and metabolism between the two species of macrophages when cells were activated with IFN-γ. The mechanisms by which IFN-γ enhances cell-intrinsic control of *M. tuberculosis* in mouse macrophages has been extensively studied. In brief, IFN-γ and TLR stimulation of mouse macrophages promotes nutrient restriction (Zhang et al., 2013), production of antimicrobial peptides (Alonso et al., 2007), and up-regulation of iNOS and NO production (Chan et al., 1992). The transcription factor hypoxia-inducible factor-1α (HIF-1α) regulates expression of a substantial portion of IFN-γ inducible genes and exists in a positive-feedback loop with iNOS to enhance macrophage activation and microbe control (Braverman et al., 2016; Braverman and Stanley, 2017). In contrast, researchers have struggled for years to detect iNOS up-regulation and NO production in human macrophages as IFN-γ treatment and TLR stimulation is insufficient (Mestas and Hughes, 2004). Some studies have suggested priming human macrophages with other cytokines such as TNFα, or IL4 and α-CD23 is necessary for iNOS up-regulation, but these claims are still fervently debated (Weinberg, 1998; Vogt and Carl, 2011). In our study, treating human macrophages with IFN-γ failed to up-regulate iNOS and did not restrict growth of *M. tuberculosis*.

Other studies have suggested that IFN-γ stimulation needs to be provided in conjunction with vitamin D to restrict *M. tuberculosis* growth (Liu et al. 2006; Selvaraj, 2011). In this model IFN-γ up-regulates expression of CYP27B1, a hydroxylase that converts the pro-vitamin D form to the active form ($1,25(OH)_2D$). $1,25(OH)_2D$ binds to vitamin D receptor (VDR), a receptor/transcription factor that regulates production of cathelicidin (Segaert, 2008; Gombart, 2009). We showed *M. tuberculosis* and *L. pneumophila* infected

human macrophages treated with IFN-γ and vitamin D up-regulate CYP27B1 and VDR. However, cathelicidin levels remain unchanged in comparison to uninfected and untreated macrophages. Additionally, IFN-γ and vitamin D activation of human macrophages failed to restrict *M. tuberculosis* growth, but did restrict *L. pneumophila*. Thus, while vitamin D pathways appear to be similarly activated during both infections, human macrophages do not up-regulate cathelicidin, and there is no correlation between bacterial restriction and differential activation.

While nitrite was detected in the supernatants of human macrophages infected with *M. tuberculosis*, it was not dependent on IFN-γ activation and did not arise from host cells. Instead, nitrite was produced by *M. tuberculosis*. Under hypoxic conditions, studies have shown that *M. tuberculosis* can use nitrate as the final electron acceptor for anaerobic respiration and nitrite is formed (Gouzy et al., 2014). Nitrate is imported into the bacteria through a transporter, which is up-regulated during hypoxia (Giffin et al., 2012). Excess nitrate is converted to nitrite via the narGHJI nitrate reductase complex and either exported out of the bacteria or further reduced to ammonium by a nitrite reductase, nirBD (Malm et al., 2009). In turn, ammonium helps protect the bacteria from acid stress. We found that infecting human macrophages with heat killed bacteria or mutants lacking a component of the narGHJI reductase significantly decreased the amount of nitrite detected. In contrast, infecting mouse bone marrow-derived macrophages with *M. tuberculosis* alone resulted in weak nitrite production from the bacteria. The majority of nitrite detected in mouse macrophages arose from NO production from host cells as the result of TLR stimulation and IFN-γ activation. While other studies have shown nitrite production from *M. tuberculosis* correlates with decreased bacterial replication and ATP consumption, *M. tuberculosis* consistently grew better in untreated human macrophages than untreated mouse macrophages, where bacteria do not produce NO_2^- (Cunningham-Bussel et al., 2013). The reasons behind *M. tuberculosis* altered metabolism in human macrophages remain unclear. While these data suggest the human macrophage environment is vastly different from a mouse macrophage and prompts the bacteria to undergo altered nitrogen metabolism, additional profiling of mouse macrophages derived from peripheral blood mononuclear cells should be performed to rule out effects potentially caused by generating macrophages from bone marrow.

Regardless of the inability to detect iNOS up-regulation and NO production in human macrophages, we knew the role of IFN-γ signaling and activation was very important. For example, research examining human families who are inherently more susceptible to mycobacteria infections identified mutations in IFN-γ and IL12 signaling pathways as being the primary cause of susceptibility (Qu et al., 2011). In this study, we showed that IFN-γ treatment of human macrophages does activate the cells and enhance mechanisms of cell intrinsic control. While IFN-γ activated human macrophages did not restrict *M.*

tuberculosis growth, they did restrict bacterial growth of *Legionella pneumophila*. Despite the remarkable differences in attenuation of the two pathogens, RNA-seq data from IFN-γ activated human macrophages infected with *M. tuberculosis* or *L. pneumophil*a were strikingly similar. IFN-γ treatment and infection with either bacteria similarly up-regulated genes canonically associated with IFN-γ signaling and other signaling pathways important for immune response to infection. The biggest differences between the data sets were in transcripts that were down-regulated by *M. tuberculosis* and up-regulated or not altered during *L. pneumophila* infection. While there were no obvious pathways identified that could account for differences in bacterial restriction, the data set requires more thorough examination.

The differences we discovered in IFN-γ activated human macrophages and their control of pathogens, or lack thereof, provided the rationale for performing a transposon-sequencing screen. When performing a screen with a slow-growing pathogen it is important to have a large dynamic range to accurately identify mutants that are attenuated for growth. By serially passaging *M. tuberculosis* mutants through macrophages three times and sequencing after each round of selection, we saw significant improvements and enrichment of the data set. Ultimately, we identified 477 *M. tuberculosis* genes that are essential for survival of the bacteria in human and mouse macrophages, with and without IFN-γ activation. Of those genes, 38 were required for growth in all conditions (Table 5). In this list of 38 genes, there are hits with intriguing putative functions, some of which have not been identified in other screens. Two uncharacterized genes (Rv1543 and 1544) belong to the same operon and are speculated to be a fatty-acyl coA reductase and ketoacyl reductase involved with fatty acid metabolism. Another, Rv0472c, is a probable transcription regulatory protein belonging to the TetR family, and could orchestrate expression of other proteins involved with survival in macrophages. Others still are simply annotated as conserved proteins (Rv0047c) and have remarkable degree of attenuation. Additional analysis of these genes, and many others, is sufficiently warranted.

Further breakdown of our dataset reveals approximately 10.7% of genes identified in our screen were essential for growth in MBMDMs only, 13.7% were only essential for growth in MBMDMs, 26.6% were conditionally essential in HDMs only, and 18.0% were essential for survival in HDMs + IFN-γ alone. However, caution must be used when interpreting classification of mutants and the percentages listed. The analysis we used to interpret the data set implemented strict cut-offs, and while Tn-seq screens are more sensitive than previous methods used to identify genes that are essential for *M. tuberculosis* survival, they are not perfect. By looking at the raw data we discovered that some of the genes identified as uniquely essential in one experimental condition were only identified as such because the statistical parameters used to determine essentiality were on the cusp of being significant in other conditions. This is a problem of every Tn-seq screen performed, but especially in slow

growing pathogens where the dynamic range for detection is inherently limited. Regardless, statistical thresholds must be used to classify gene essentiality. To compensate for this, careful consideration of the raw data is necessary for choosing potential mutants for validation. Ultimately this data set is very illuminating, and will be used to spur new hypotheses as to how *M. tuberculosis* survives in the macrophage.

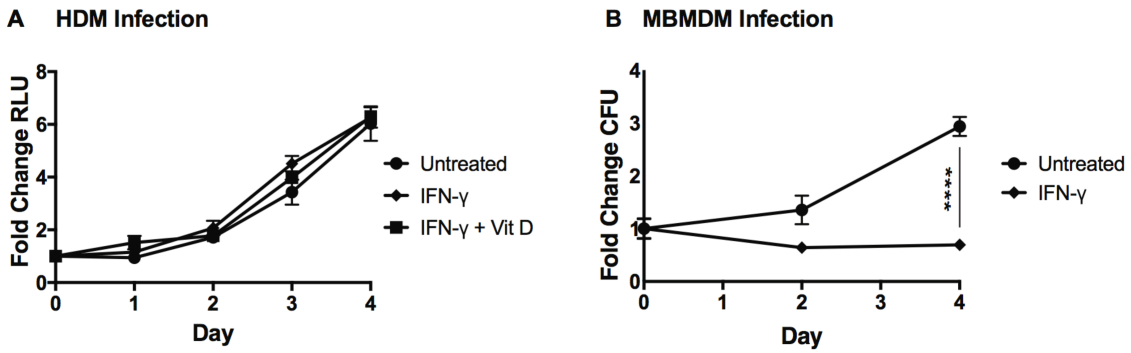

Figure 1. IFN-γ stimulation restricts *M. tuberculosis* growth in mouse macrophages but not human macrophages**. A.** Human macrophages were pre-treated with IFN-γ, IFN-γ and vitamin D, or left untreated and infected (MOI 0.5) with a luminescent strain of *M. tuberculosis*. Luminescent measurements were taken immediately following phagocytosis and every 24 hours thereafter. **B.** Mouse bone marrow derived macrophages were pre-treated with IFN-γ or left untreated and infected with wild-type *M. tuberculosis* (MOI 1). CFU were enumerated immediately following phagocytosis and 2 and 4 days post infection. **A** and **B** are representative of over 3 experiments. The p values were determined using an unpaired t test. **** $p < 0.0001$.

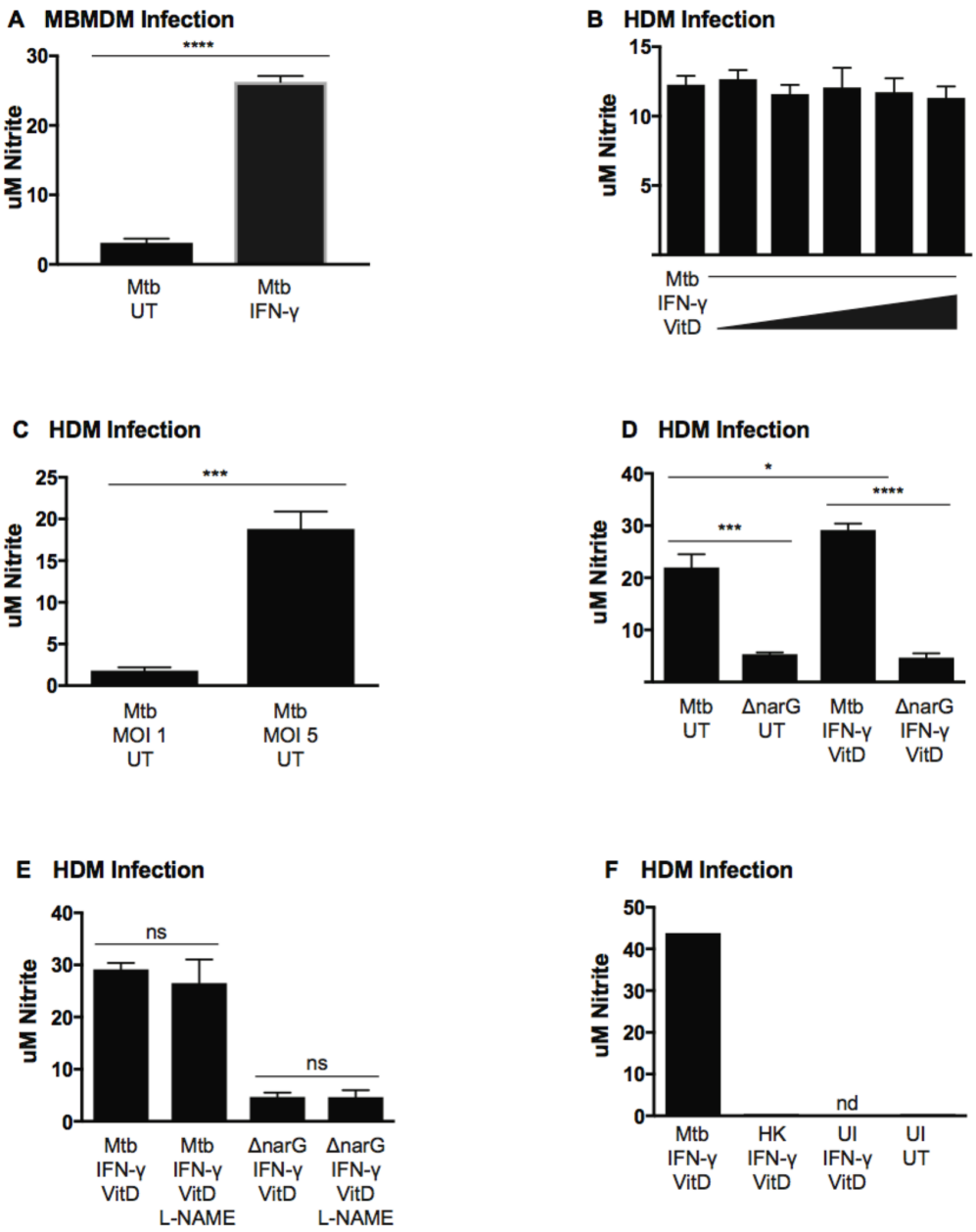

Figure 2. Nitrite detected during human macrophage infection is produced by *M. tuberculosis*. Griess assays measuring nitrite production under the following conditions: **A.** 24 hours post infection in untreated (UT) mouse bone marrow macrophages and macrophages stimulated with IFN-γ; MOI 5. **B.** 48 hours post infection of *M. tuberculosis* infected human macrophages, with a dose response of IFN-γ (0, 2.5, 5, 10, 20, 40 ng/mL); MOI 1. **C.** 24 hours post infection in untreated human macrophages; MOI 1 and MOI 5. **D.** 48 hours post infection of untreated (UT) or IFN-γ and vitamin D stimulated human macrophages infected with wild type or ΔnarG *M. tuberculosis*; MOI 5. **E.** 48 hours post infection of IFN-γ and vitamin D stimulated macrophages with and without presence of iNOS inhibitor (L-NAME; 100 uM). Cells were infected with wild-type of ΔnarG *M. tuberculosis* at MOI 5. **F.** 24 hours post infection of human macrophages infected with wild-type *M. tuberculosis*, heat killed (HK) *M. tuberculosis*, or uninfected (UI); MOI 5. **A-F** are representative of 2 or more experiments. The p values were determined using an unpaired t test. *p<.05, ***p<0.001, ****p<0.0001, ns: not significant.

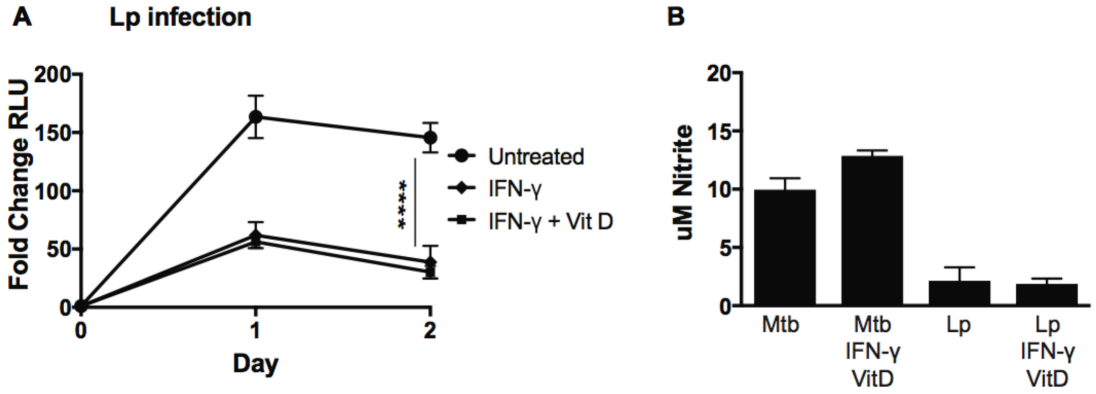

Figure 3. IFN-γ stimulated human macrophages restrict growth of *L. pneumophila*. **A.** Human macrophages were pre-treated with IFN-γ, IFN-γ and vitamin D, or left untreated and infected with a luminescent strain of *L. pneumophila* (LP02 ΔflaA; MOI 0.5). Luminescent measurements were taken immediately following phagocytosis and every 24 hours thereafter. **B.** Griess assay measurements of nitrite production in untreated or IFN-γ and vitamin D stimulated human macrophages 24 hours post-infection. Macrophages were infected with *M. tuberculosis* or *L. pneumophila* (Lp); MOI 1. **A** and **B** are representative of three experiments. The p values were determined using an unpaired t test. ****p<0.0001

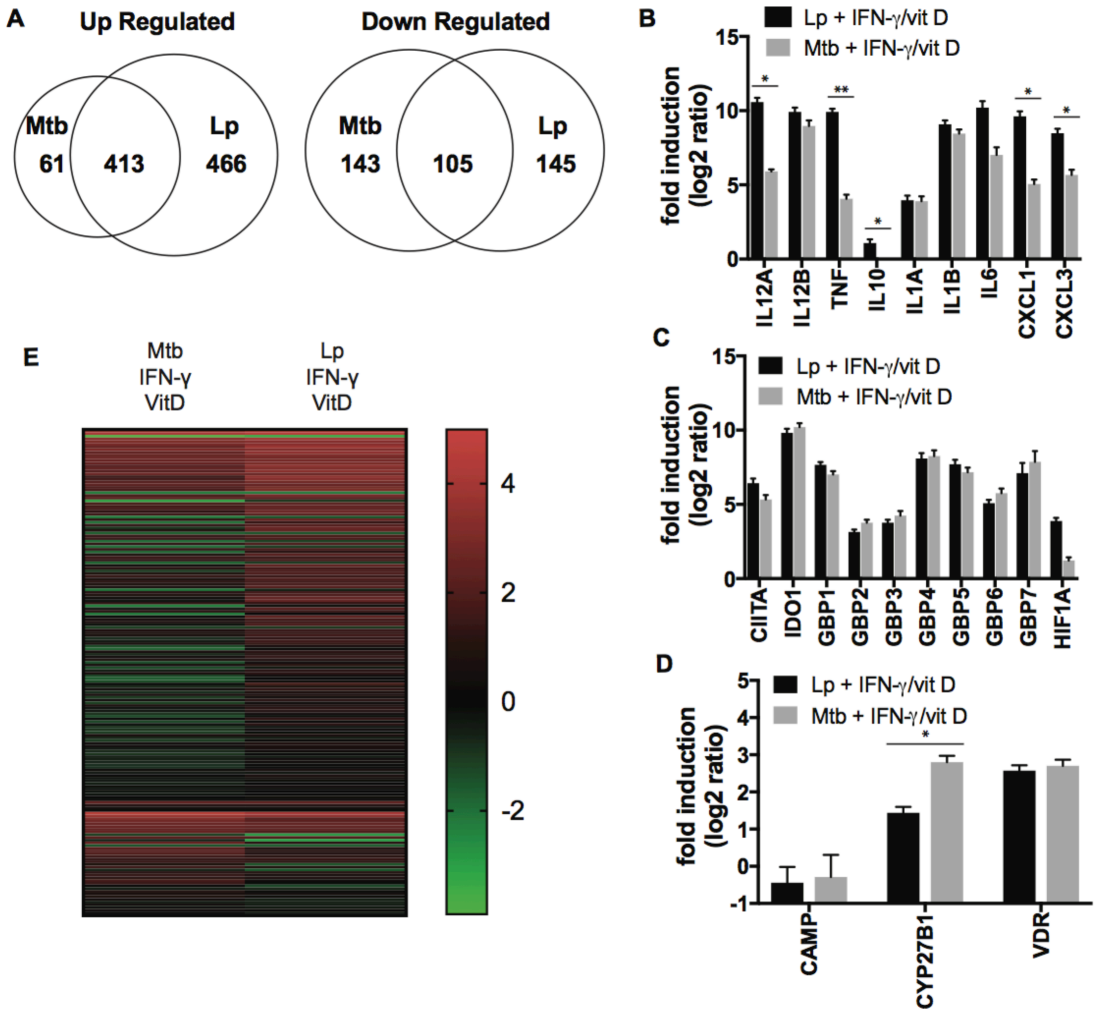

Figure 4. IFN-γ stimulated human macrophages are similarly activated during infection with *M. tuberculosis* and *L. pneumophila*. **A.** Venn diagram of statistically significant RNA-seq data showing overlap of genes differentially regulated during *M. tuberculosis* and *L. pneumophila* infection of human macrophages activated with IFN-γ and vitamin D. Data are normalized to uninfected and untreated human macrophages. Only showing data with p value ≤ 0.05; 3 ≤ log2 fold change ≤ -3. RNA-seq data showing fold induction of inflammatory cytokines and chemokines (**B**), IFN-γ regulated genes (**C**), or vitamin D regulated genes (**D**) during *M. tuberculosis* and *L. pneumophila* infection of IFN-γ and vitamin D stimulated human macrophages relative to untreated and uninfected macrophages. **E.** Heat map depicting activation z-score predictions for pathways activated during *M. tuberculosis* and *L. pneumophila* infection of IFN-γ and vitamin D stimulated human macrophages. Activation z-score prediction values generated by Ingenuity Pathway Analysis of RNA-seq transcripts. **B-D** are representative of three experiments. The p values were determined using an unpaired t test. *p<0.05, **p<0.01, ****p<0.0001

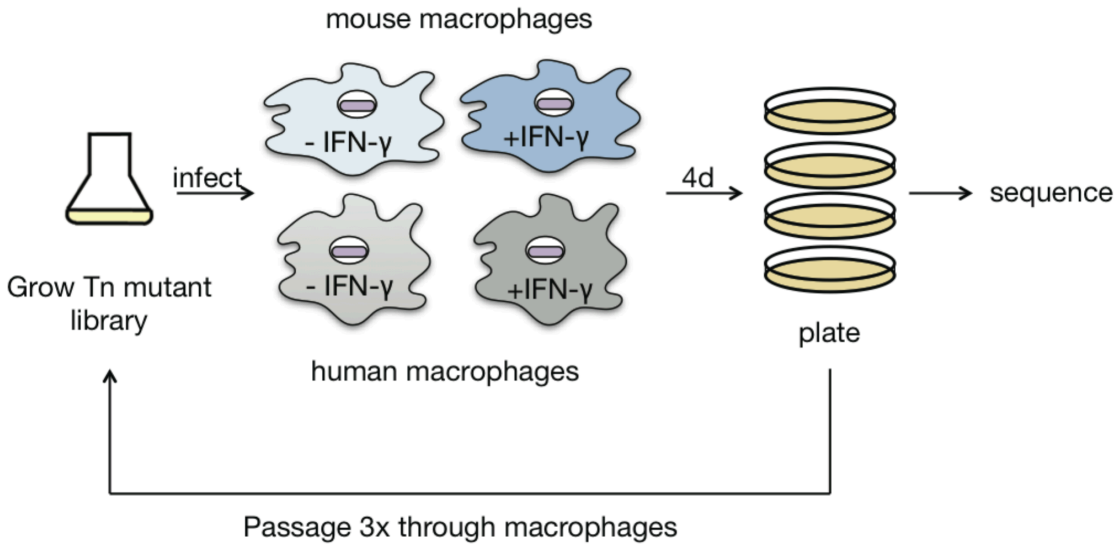

Figure 5. Experimental design for Tn-seq screen. A transposon mutant library in *M. tuberculosis* was used to infect human and mouse macrophages that had been activated with IFN-γ or left untreated. At the end of a 4-day infection, macrophages were lysed and surviving bacteria were plated on 7H10 agar. Following growth of bacteria, a portion of mutants were prepared for Illumina sequencing and another fraction were re-passaged through macrophages. Mutants were serially passaged through macrophages a total of three times, with sequencing performed after each passage. The screen was performed in triplicate.

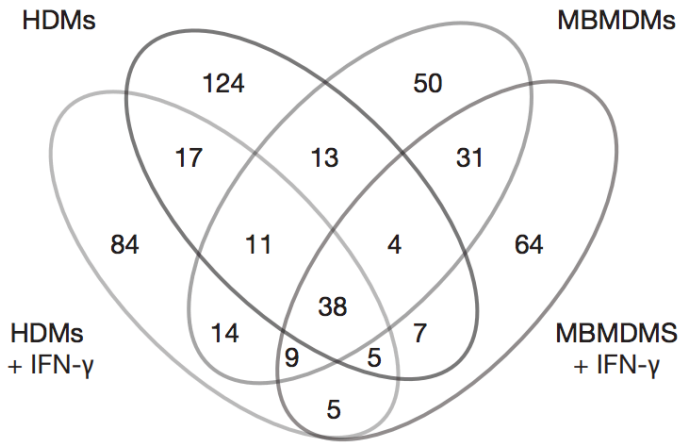

Figure 6. Result summary of *M. tuberculosis* genes essential for survival in macrophages. Venn diagram depicting overlap in *M. tuberculosis* genes found to be essential for bacterial survival in human and mouse macrophages activated with +/-IFN-γ. Genes determined essential by p value≤ 0.05 and log2 fold change ≤ -1.

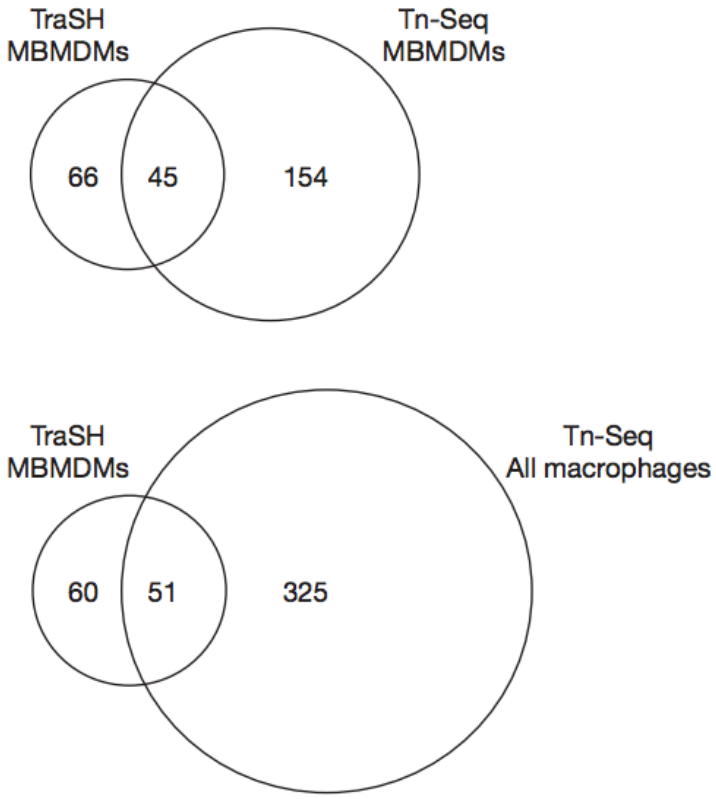

Figure 7. Comparison of statistically significant hits identified in macrophage Tn-Seq and TraSH screen. A venn diagram depicting overlap in genes identified in our study for survival of *M. tuberculosis* in mouse macrophages (upper) or human and mouse macrophages (lower) with genes identified in a previous transposon site hybridization screen performed in mouse macrophages. Genes determined essential by p value ≤ 0.05 and log 2 FC ≤ -1.3.

Table 1: Activation z-score predictions for pathways activated during *M. tuberculosis* and *L. pneumophila* infection of human macrophages. Table sorted by most differentially regulated pathways

Canonical Pathway	**Mtb + IFNγ/VitD z-score**	**Lp + IFNγ/VitD z-score**
Estrogen-mediated S-phase Entry	-2.1	1.3
Wnt/Ca+ pathway	-0.9	2.5
14-3-3-mediated Signaling	-1.9	1.1
Gαi Signaling	-1.0	1.8
Mouse Embryonic Stem Cell Pluripotency	-0.2	2.4
Cell Cycle Regulation by BTG Family Proteins	-0.4	2.1
Cell Cycle: G1/S Checkpoint Regulation	0.8	-1.6
PI3K Signaling in B Lymphocytes	-0.6	-3.0
Aldosterone Signaling in Epithelial Cells	-3.3	-1.0
Mitotic Roles of Polo-Like Kinase	-2.3	0.0
Basal Cell Carcinoma Signaling	0.0	2.3
Cyclins and Cell Cycle Regulation	-2.4	-0.2
NRF2-mediated Oxidative Stress Response	-0.2	1.9
April Mediated Signaling	0.3	2.4
TGFβ Signaling	-0.8	1.3
UVC-Induced MAPK Signaling	-0.4	1.5
Sonic Hedgehog Signaling	-1.3	0.6
PCP pathway	0.5	2.4
B Cell Activating Factor Signaling	1.5	3.4
p70S6K Signaling	-1.8	0.0
PPARα/RXRα Activation	-1.2	-2.9
FcγRIIB Signaling in B Lymphocytes	-0.7	1.1
Glioma Signaling	-1.4	0.3
Rac Signaling	-0.6	1.1
α-Adrenergic Signaling	-1.3	0.4
UVB-Induced MAPK Signaling	-1.7	0.0
Role of NFAT in Cardiac Hypertrophy	-1.4	0.3
Neurotrophin/TRK Signaling	0.0	1.6
P2Y Purigenic Receptor Signaling Pathway	-0.7	0.9
Actin Nucleation by ARP-WASP Complex	1.6	3.2
cAMP-mediated signaling	-0.8	0.7
Macropinocytosis Signaling	-1.1	0.4
LPS-stimulated MAPK Signaling	0.9	2.4
Fcγ Receptor-mediated Phagocytosis in Macrophages and Monocytes	-1.1	0.3
MIF-mediated Glucocorticoid Regulation	2.5	1.1
Cardiac Hypertrophy Signaling	-0.3	1.1

CREB Signaling in Neurons	-2.0	-0.6
nNOS Signaling in Neurons	1.4	0.0
B Cell Receptor Signaling	1.2	2.6
LPS/IL-1 Mediated Inhibition of RXR Function	1.6	0.2
Wnt/β-catenin Signaling	0.8	2.2
Glioblastoma Multiforme Signaling	1.2	2.5
Thrombopoietin Signaling	-0.3	1.0
Endothelin-1 Signaling	-0.9	0.4
Melanocyte Development and Pigmentation Signaling	-1.3	0.0
Leptin Signaling in Obesity	0.0	-1.3
p53 Signaling	0.7	2.0
Role of NFAT in Regulation of the Immune Response	0.0	1.3
Prolactin Signaling	-1.3	0.0
UVA-Induced MAPK Signaling	-0.2	1.1
fMLP Signaling in Neutrophils	-0.9	0.3
Activation of IRF by Cytosolic Pattern Recognition Receptors	2.0	3.3
Role of Pattern Recognition Receptors in Recognition of Bacteria and Viruses	2.0	3.3
Tec Kinase Signaling	1.7	2.9
Cholecystokinin/Gastrin-mediated Signaling	2.4	3.7
VDR/RXR Activation	2.3	3.5
Lymphotoxin β Receptor Signaling	0.8	1.9
mTOR Signaling	-1.1	0.0
Ephrin Receptor Signaling	2.1	1.0
Granzyme B Signaling	0.8	1.9
Role of CHK Proteins in Cell Cycle Checkpoint Control	2.1	1.0
CD40 Signaling	0.9	1.9
Chemokine Signaling	-0.4	0.6
NF-κB Signaling	1.8	2.8
Inhibition of Angiogenesis by TSP1	0.4	1.4
Renal Cell Carcinoma Signaling	0.6	1.6
Protein Kinase A Signaling	0.5	-0.5
IL-3 Signaling	-1.3	-0.4
GNRH Signaling	-1.1	-0.1
Paxillin Signaling	-0.7	0.2
PI3K/AKT Signaling	3.0	2.1
Pancreatic Adenocarcinoma Signaling	2.0	1.0
OX40 Signaling Pathway	0.6	1.5
NGF Signaling	1.9	2.8
Apoptosis Signaling	0.4	-0.5
Induction of Apoptosis by HIV1	0.9	1.8

ErbB4 Signaling	-0.9	0.0
VEGF Family Ligand-Receptor Interactions	-0.5	0.4
HMGB1 Signaling	4.1	5.0
eNOS Signaling	-2.0	-1.1
Role of BRCA1 in DNA Damage Response	-0.6	0.2
Cardiac β-adrenergic Signaling	-0.7	-1.5
HGF Signaling	0.4	1.2
Sphingosine-1-phosphate Signaling	0.4	1.2
IL-8 Signaling	1.4	0.6
Growth Hormone Signaling	-2.0	-1.2
Sperm Motility	-0.8	0.0
Angiopoietin Signaling	-0.8	0.0
FLT3 Signaling in Hematopoietic Progenitor Cells	1.5	2.3
Melatonin Signaling	-1.8	-1.0
PAK Signaling	0.9	0.2
Signaling by Rho Family GTPases	0.6	1.3
Huntington's Disease Signaling	-2.2	-1.5
Tumoricidal Function of Hepatic Natural Killer Cells	1.6	2.3
FGF Signaling	0.7	1.4
Telomerase Signaling	0.8	1.5
TNFR1 Signaling	2.3	3.0
Death Receptor Signaling	1.4	2.0
ATM Signaling	1.5	0.9
Neuregulin Signaling	0.0	0.7
Dopamine-DARPP32 Feedback in cAMP Signaling	-1.0	-0.3
Renin-Angiotensin Signaling	-0.2	0.4
IL-6 Signaling	3.2	3.9
CD28 Signaling in T Helper Cells	1.2	1.9
Acute Myeloid Leukemia Signaling	2.1	2.7
ILK Signaling	1.6	2.3
Gαs Signaling	1.0	1.6
IL-2 Signaling	0.6	1.1
TWEAK Signaling	0.8	1.3
TREM1 Signaling	4.6	4.0
Notch Signaling	2.4	1.9
CXCR4 Signaling	1.1	1.7
PPAR Signaling	-3.9	-3.4
Regulation of eIF4 and p70S6K Signaling	-0.5	0.0
MIF Regulation of Innate Immunity	2.7	2.2
ERK/MAPK Signaling	-0.2	0.4
Complement System	0.6	1.2

Colorectal Cancer Metastasis Signaling	2.5	3.0
Type I Diabetes Mellitus Signaling	2.4	2.9
AMPK Signaling	0.8	0.3
Glioma Invasiveness Signaling	1.8	2.3
SAPK/JNK Signaling	1.1	0.7
JAK/Stat Signaling	0.6	1.1
Gαq Signaling	1.3	1.7
Role of IL-17F in Allergic Inflammatory Airway Diseases	2.8	3.3
iCOS-iCOSL Signaling in T Helper Cells	1.1	1.6
Role of NANOG in Mammalian Embryonic Stem Cell Pluripotency	0.3	0.7
Ceramide Signaling	1.4	1.8
G Beta Gamma Signaling	0.0	-0.4
Dendritic Cell Maturation	4.1	4.5
PDGF Signaling	1.0	1.4
p38 MAPK Signaling	1.4	1.8
IL-1 Signaling	1.5	1.2
Synaptic Long Term Potentiation	-0.2	0.2
STAT3 Pathway	0.2	0.5
Phospholipase C Signaling	0.6	0.9
Type II Diabetes Mellitus Signaling	1.3	1.6
Aryl Hydrocarbon Receptor Signaling	-0.3	0.0
4-1BB Signaling in T Lymphocytes	2.5	2.8
Role of PI3K/AKT Signaling in the Pathogenesis of Influenza	-0.3	0.0
Antiproliferative Role of Somatostatin Receptor 2	0.0	0.3
Calcium Signaling	0.4	0.6
PTEN Signaling	-1.5	-1.8
Nitric Oxide Signaling in the Cardiovascular System	-0.4	-0.2
CD27 Signaling in Lymphocytes	2.1	1.9
Oncostatin M Signaling	2.5	2.3
iNOS Signaling	2.2	2.4
Antioxidant Action of Vitamin C	-1.7	-1.5
Eicosanoid Signaling	-0.4	-0.6
Acute Phase Response Signaling	2.5	2.3
RhoGDI Signaling	0.4	0.2
Production of Nitric Oxide and Reactive Oxygen Species in Macrophages	3.7	3.5
CDK5 Signaling	-0.5	-0.7
EGF Signaling	0.6	0.4
HIPPO signaling	0.6	0.8
PKCθ Signaling in T Lymphocytes	2.6	2.8

IGF-1 Signaling	-0.5	-0.4
Fc Epsilon RI Signaling	0.0	0.2
Role of RIG1-like Receptors in Antiviral Innate Immunity	2.9	3.1
Toll-like Receptor Signaling	3.0	3.1
Calcium-induced T Lymphocyte Apoptosis	-1.2	-1.0
Relaxin Signaling	-0.2	-0.4
BMP signaling pathway	2.3	2.2
Corticotropin Releasing Hormone Signaling	-0.7	-0.5
GM-CSF Signaling	1.1	1.0
IL-17A Signaling in Airway Cells	1.3	1.2
PEDF Signaling	0.8	0.9
Cell Cycle: G2/M DNA Damage Checkpoint Regulation	1.4	1.3
RANK Signaling in Osteoclasts	1.3	1.4
LXR/RXR Activation	-2.3	-2.3
Thrombin Signaling	1.3	1.3
Neuropathic Pain Signaling In Dorsal Horn Neurons	-0.4	-0.3
Integrin Signaling	0.6	0.6
TNFR2 Signaling	2.1	2.2
Hypoxia Signaling in the Cardiovascular System	2.6	2.7
Leukocyte Extravasation Signaling	1.4	1.5
Role of JAK1, JAK2 and TYK2 in Interferon Signaling	0.4	0.4
IL-9 Signaling	1.0	1.0
Interferon Signaling	2.4	2.4

Table 2: Essentiality predictions for genes in *H37Rv M. tuberculosis*

Number of genes	Percentage	Prediction
583	14.5	Essential
2860	71	Non-Essential
262	6.5	Short
331	8	Uncertain (Domain Essential?)

Table 3: Number of conditionally essential genes as determined by different statistical parameters

	MBMDMs		MBMDMs +IFN-γ		HDMs		HDMs +IFN-γ	
Passage	Padj	Pval + FC	Padj	Pval + FC	Padj	Pval + FC	Padj	Pval + FC
1	25	107	44	83	17	81	12	94
2	31	135	65	120	26	167	21	179
3	51	238	92	225	45	295	35	239

Table 4: Statistical parameters used to classify essentiality change as a mutant is passaged through macrophages

Passage	Gene	log2 FC	Pval	Padj
1	Rv2243	-0.74	0.4542	1
2	Rv2243	-2.96	0.0208	0.5711
3	Rv2243	-5.4	0.0015	0.0931

Table 5: Genes conditionally essential for survival in all macrophage conditions tested

Gene	Description	Protein
Rv0047c	Conserved protein	Rv0047c
Rv0167	ABC transporter permease	yrbE1A
Rv0168	ABC transporter permease	yrbE1B
Rv0169	MCE-family protein MCE1A	mce1A
Rv0170	Mammalian cell entry protein	mce1B
Rv0171	Mammalian cell entry protein	mce1C
Rv0172	Mammalian cell entry protein	mce1D
Rv0173	Possible Mce-family lipoprotein LprK (Mce-family lipoprotein Mce1E)	lprK
Rv0174	Mammalian cell entry protein	mce1F
Rv0175	Probable conserved Mce associated membrane protein	Rv0175
Rv0176	Membrane protein	Rv0176
Rv0177	Mammalian cell entry protein	Rv0177
Rv0178	Mammalian cell entry protein	Rv0178
Rv0472c	Uncharacterized HTH-type transcriptional regulator Rv0472c	Rv0472c
Rv0541c	Membrane protein	Rv0541c
Rv0642c	Hydroxymycolate synthase MmaA4	mmaA4
Rv0643c	Methoxy mycolic acid synthase MmaA3	mmaA3
Rv0655	Probable ribonucleotide transport ATP-binding protein mkl	mkl
Rv0928	Phosphate-binding protein PstS 3	pstS3
Rv1086	(2Z,6E)-farnesyl diphosphate synthase	Rv1086
Rv1130	2-methylcitrate dehydratase	prpD
Rv1131	2-methylcitrate synthase	prpC
Rv1364c	Uncharacterized protein Rv1364c	Rv1364c
Rv1411c	Lipoprotein LprG	lprG
Rv1543	Uncharacterized oxidoreductase Rv1543	Rv1543
Rv1544	Ketoacyl reductase	Rv1544
Rv1780	Conserved protein	Rv1780
Rv2173	Geranylgeranyl pyrophosphate synthase	idsA2
Rv2224c	Carboxylesterase A	caeA
Rv2594c	Crossover junction endodeoxyribonuclease RuvC	ruvC
Rv2967c	Pyruvate carboxylase	pca
Rv3311	Conserved protein	Rv3311
Rv3540c	Lipid-transfer protein	ltp2
Rv3542c	Uncharacterized protein	Rv3542c
Rv3550	Enoyl-CoA hydratase	echA20
Rv3551	Putative CoA-transferase subunit alpha Rv3551	Rv3551
Rv3568c	Iron-dependent extradiol dioxygenase	hsaC
Rv3569c	4,5:9,10-diseco-3-hydroxy-5,9,17-trioxoandrosta-1(10),2-diene-4-oate hydrolase	hsaD

Table 6: Essentiality predictions for three example genes

Condition	Gene	Description	log2 FC	Pval	Padj	Prediction
HDMs	Rv3541c	Hypothetical protein	-3.48	0.0107	0.2776	Essential
HDMs + IFN-γ	Rv3541c	Hypothetical protein	-7.9	0.0011	0.1009	Essential
MBMDMs	Rv3541c	Hypothetical protein	-8	0.0004	0.0359	Essential
MBMDMs + IFN-γ	Rv3541c	Hypothetical protein	-2.46	0.0572	0.6559	Not Essential
HDMs	Rv3868	ESX-1 protein EccA1	-1.27	0.0009	0.0685	Essential
HDMs + IFN-γ	Rv3868	ESX-1 protein EccA1	-0.9	0.0176	0.446	Not Essential
MBMDMs	Rv3868	ESX-1 protein EccA1	-1.66	0	0	Essential
MBMDMs + IFN-γ	Rv3868	ESX-1 protein EccA1	-0.72	0.0371	0.5231	Not Essential
HDMs	Rv1411c	lipoprotein LprG	-4.2	0.0108	0.2776	Essential
HDMs + IFN-γ	Rv1411c	lipoprotein LprG	-5.4	0.0032	0.1819	Essential
BMDMs	Rv1411c	lipoprotein LprG	-7.15	0.0001	0.0112	Essential
BMDMs + IFN-γ	Rv1411c	lipoprotein LprG	-6.6	0	0	Essential

Chapter 3

Bacterial nanocompartments protect *Mycobacterium tuberculosis* from oxidative and acid stress

3.1 Abstract

Mycobacterium tuberculosis forms a replicative niche inside phagocytic cells such as macrophages and neutrophils. As members of the innate immune system, macrophages and neutrophils undergo a respiratory burst upon infection and produce reactive oxygen species (ROS) to combat infection. Despite this, *M. tuberculosis* is relatively resistant to ROS. In this study we demonstrate that *M. tuberculosis* produces a proteinaceous organelle known as a nanocompartment to protect the bacteria from oxidative and acid stress. *M. tuberculosis* nanocompartments are comprised of an encapsulin protein that forms a hollow shell. We discovered a dye-decoloring peroxidase (DypB) is packaged inside of the nanocompartment, and the peroxidase displays enhanced enzymatic activity at acidic pH levels. *M. tuberculosis* mutants lacking a functional nanocompartment are attenuated when exposed to oxidative and acid stress. Additionally, we show that packaging of the DypB inside of the nanocompartment is essential to confer complete protection to the bacteria when exposed to these stressors. Oxidative stress and acidic pH are hallmarks of the phagolysosome environment in macrophages. In this study we show that nanocompartments are not only essential for bacterial survival in artificial conditions emulating phagolysosomes, but they are essential for survival within the macrophage as well.

3.2 Introduction

Mycobacterium tuberculosis continues to be a significant global problem as it infects one-third of the world and kills more people annually than any single infectious disease (WHO Global Tuberculosis Report, 2018). Upon infection, *M. tuberculosis* is phagocytosed by alveolar macrophages. Newly infected macrophages secrete TNFα and an amalgam of other cytokines that recruit immune cells to the infection site (Algood et al., 2003; Russell, 2006). Among the first cells to arrive are neutrophils. While short-lived, neutrophils are abundant and functionally robust. They phagocytose bacteria and amplify the cytokine storm to recruit monocytes and lymphocytes to the lungs. During bacterial infection, both macrophages and neutrophils undergo a respiratory burst that generates reactive oxygen species such as superoxide, hydrogen peroxide, hydroperoxyl radicals, and hypochlorous acid. The primary driver of ROS production is the NADPH oxidase, which assembles on the phagosome membrane of activated macrophages and neutrophils (Chan et al., 1992; Nathan, 2006).). While NADPH oxidase specifically catalyzes the production of superoxide from molecular oxygen, superoxide is converted to other ROS with more potent levels of reactivity. Ultimately, NADPH oxidase initiates production of the wide assortment of ROS that react with proteins, lipids, DNA, RNA, etc. and kill invading pathogens (Bedard and Krause, 2007).

Interestingly, *M. tuberculosis* is capable of mitigating the effects of ROS generated by the host (Chan et al., 1991; Newton et al., 2008). In one of the seminal studies to examine this, researchers infected $p47^{phox}$ (a component of the NADPH oxidase complex) knockout mice with *M. tuberculosis* (Cooper et al., 2000). Humans lacking functional NADPH oxidase are extraordinarily susceptible to bacterial and fungal infections such as *Salmonella* species, *Aspergillus fumugatis*, and some studies even report they are susceptible to members of the *Mycobacterium* genus (Bustamante et al., 2007; Lee et al., 2008). However, deletion of NADPH oxidase in mice infected with *M. tuberculosis* resulted in a small and transient increase in infectious burden that was ultimately resolved at the onset of adaptive immunity (Cooper et al., 2000). These data suggested that while ROS may play a role in the early stages of control, NADPH oxidase is ultimately dispensable for control of *M. tuberculosis* infection.

Mycobacterium tuberculosis has approximately 15 genes that encode proteins to combat ROS stress, including a catalase-peroxidase (KatG), two superoxide dismutases (SodA, SodC), and a variety of other peroxidases. Of the peroxidases encoded by *M. tuberculosis*, one is a dye-decoloring peroxidase (Rv0799c; DypB). Dyp proteins are a family of heme-peroxidases with remarkably low homology to other peroxidases (Chen and Li, 2016). Mostly noted for their ability to degrade lignin, anthraquinone and other phenol containing dyes, a study in *Halobacterium salinarum* identified dye-decoloring peroxidases as being important for combatting extreme levels of ROS (Kaur et al., 2010). Interestingly, members of this family of peroxidases have reported acidic pH optimums (~3-5), which suggests DypB may function in environments where other peroxidases are inactive (Sugano et al., 2000, Sugano et al., 2007; Uchida et al., 2015).

Another unique feature of the DypB gene in *M. tuberculosis* is its position immediately upstream of Rv0798c, a gene that encodes an encapsulin shell protein, Cfp29 (culture filtrate protein, 29 kDa) (Contreras et al., 2014). Encapsulin proteins assemble to form proteinaceous organelles approximately 25-35 nm in diameter (Giessen and Silver, 2017; Nichols et al., 2017; Cassidy-Amstutz et al., 2016). This organelle is a hollow nanocompartment that packages cargo proteins inside. Most cargo proteins are encoded by genes immediately upstream of the encapsulin shell gene and have a targeting peptide sequence on the C-terminal tail that facilitates loading into the nanocompartment (Cassidy-Amstutz et al., 2016). Although, it has been speculated that secondary cargo proteins found outside of the operon may be loaded into the nanocompartment as well (Giessen and Silver, 2017). Identity of cargo proteins vary, but most putative nanocompartment structures are thought to package dye-decoloring peroxidases and ferritin-like proteins (Giessen et al., 2017; Nichols et al., 2017). Small pores ~5 Å in size are located at each fold of symmetry in the encapsulin shell. The pores vary in chemical nature: one subset

is negatively charged, another is uncharged and gated by histidine residues that coordinate a metal ion, and the final group is positively charged in some species and neutral in others (Sutter et al., 2008; Nichols et al., 2017). Regardless, the pores allow for exchange of small molecules and metabolites and may alter the functional concentration of cargo protein substrates or protect the bacteria from toxic reactions occurring within the nanocompartment.

Nanocompartments were first discovered in 2007 and since then bioinformatic analysis has identified over 900 putative nanocompartment operons in bacteria and archea (Giessen and Silver, 2017). Despite the widespread prevalence of theses organelles, endogenous nanocompartments have been purified in only a few bacterial species including *Thermotoga maritima*, *Rhodococcus jostii*, and *Myxococcus xanthus* (Cassidy-Amstutz et al., 2017; McHugh et al, 2014; Rahmanpour and Bugg, 2013). From the few studies that have been performed, some interesting information regarding the characteristics and function of nanocompartments can be gleaned. A study conducted by Cassidy-Amstutz et al. reported nanocompartments from *T. maritima* are remarkably resistant to acid, protease, and heat stressors (2017). The study conducted in *M. xanthus* is the only study that addresses the endogenous functions of nanocompartments and their cargo proteins (2 ferritin like proteins). In this study, they found amino acid starvation of the bacteria induces sporulation and increased production of encapsulin shell proteins. Additionally, they discovered deleting the encapsulin shell gene results in enhanced susceptibility of the bacteria to H_2O_2 stress (McHugh et al., 2014).

To date, there has been one study that has looked at the *M. tuberculosis* nanocompartment. Contreras et al. heterologously over-expressed the encapsulin shell protein, Cfp29, and three potential cargo proteins in *E. coli* (2014). They reported packaging of DypB, FolB (a protein involved with folate biosynthesis), and BfrB (a ferritin protein). They also confirmed the identity of DypB as a heme-binding peroxidase capable of oxidizing ABTS and guiacol. While informative, the study did not address if *M. tuberculosis* endogenously produces nanocompartments or comment on whether nanocompartments are important for virulence of the bacteria.

In this study we show that *M. tuberculosis* produces a functional nanocompartment that packages DypB as a cargo protein. DypB functions as a peroxidase that is preferentially active at low pH levels. Strikingly, mutants lacking components of the nanocompartment are hypersusceptible to damage mediated by oxidative stress at low pH. While DypB expression alone is sufficient to confer partial protection to bacteria exposed to low pH and ROS, we show DypB must be packaged inside of the encapsulin shell to confer full protection. During infection of host macrophages, bacteria are subjected to similar low pH and oxidative stress in the phagolysosome suggesting a role for nanocompartments during macrophage infection. Indeed, we demonstrate that

nanocompartment mutants are attenuated in host macrophages thereby providing the most characterized physiological role of nanocompartments to date.

3.3 Materials and Methods

3.3.1 Ethics statement

All procedures involving the use of mice were approved by the University of California, Berkeley Institutional Animal Care and Use Committee (protocol no. R353-1113B). All protocols conform to federal regulations, the National Research Council's *Guide for the Care and Use of Laboratory Animals*, and the Public Health Service's *Policy on Humane Care and Use of Laboratory Animals*.

3.3.2 Mycobacterium tuberculosis bacterial strains and plasmids

The *M. tuberculosis* strain H37Rv was used for all experiments. The transposon mutant Tn::DypB was from The Broad Institute (Cambridge, MA). The ΔOperon, ΔCfp29, and ΔDypB strains were made by homologous recombination using the pMSG361 vector (Rosenberg et al., 2015). For genetic complementation studies, the region encoding GFP and KanR in pUV15tetORm (Guo et al., 2007) was substituted via GoldenGate cloning with open reading frames for Rv0798c, Rv0799c, and the whole operon (Rv0798-99c). Expression of the complementation constructs was induced with anhydrotetracycline (200ng/mL). To measure redox homeostasis, strains were transformed with pMV762-mrx1-roGFP2, which was a gift from A. Singh (Bhaskar et al., 2014).

3.3.3 M. tuberculosis bacterial cell culture

For infections*, M. tuberculosis* was grown to mid-log phase (OD_{600} nm 0.5-1.0) in Middlebrook 7H9 liquid media supplemented with 10% albumin-dextrose-saline, 0.4% glycerol, and 0.05% Tween-80 or on solid 7H10 agar plates supplemented with Middlebrook OADC (BD Biosciences) and 0.4% glycerol. When specified, Tween-80 was substituted with 0.05% Tyloxapol, and 10% albumin-dextrose-saline was prepared with fatty acid free BSA. Sauton's media was prepared as specified by Larsen et al. (2007) except Tyloxapol was used instead of Tween-80.

3.3.4 ABTS Assay

Purification of Apo-SUMO-DypB and ABTS assay were performed by Rob Nichols and are reported here with permission. Apo-SUMO-DypB (538 nM) peroxidase activity was measured using ABTS (480 nM) as a substrate in the presence of H_2O_2 at pH 3.5-6.5. The reaction was allowed to proceed for 20 minutes and the absorbance was measured at 420 nm.

3.3.5 Protein Purification

For each purification, 1.5 L of M. tuberculosis was grown to mid-log phase in standard 7H9, pelleted and washed with PBS. Bacteria were pelleted and lysed by bead beating. Per 50 mL of lysis buffer, PBS was supplemented with 50 mg lysozyme, 20 U DNaseI, 100 ug RNase A, and 1 mM PMSF. Lysates were passaged twice through 0.2 µm filters before removal from the BSL3. Protein purifications were performed by Caleb Cassidy-Amstutz and are reported here with permission. Clarified lysates were prepared by centrifugation at 20,000 x g for 20 minutes in a JA-20 rotor. Following clarification, lysates were layered onto top of a 38% sucrose gradient and centrifuged for 18 hours at 100,000 RPM in a type 50.2 Ti rotor. The supernatant was discarded and the pellet was re-suspended in 200 µL of PBS. Re-suspended pellets were layered on top of a10-50% sucrose gradient and centrifuged for 21 hours at 100,000 x g in a SW 41 Ti rotor. The gradient was fractionated and aliquots from each fraction were analyzed by SDS-PAGE for the presence of CFP29.

3.3.6 Polyacrylamide Gel Electrophoresis

PAGE analysis was performed by Caleb Cassidy-Amstutz and reported here with permission. Samples were run on Criterion TGX 4-20% gels and stained with GelCode Blue for 30 minutes at room temperature. Gels were de-stained for 2 hours at room temperature with diH_2O. Imaging was performed with a ChemiDoc MP Imaging System.

3.3.7 Electron Microscopy

Electron microscopy was performed by Caleb Cassidy-Amstutz and reported here with permission. Following adsorption onto a thin carbon grid, CFP29 was stained with a 1% (w/v) uranyl acetate solution. Films were washed with water twice and dehydrated. Grids were examined with a JEOL 12000EX transmission electron microscope, and images were captured with a charge-coupled device (CCD) camera.

3.3.8 Exposure to oxidative and pH stress

M. tuberculosis was grown to mid-log phase in 7H9 media. Bacteria were diluted to OD_{600} nm 0.1 in 10 mL of specified media at pH 4.5 or 6.5. H_2O_2 was added to bacterial cultures at specified concentrations. Bacteria were incubated with stressors for 24 or 72 hours and the bacterial CFU were enumerated by diluting bacteria in PBS with 0.05% Tween-80 and plating serial dilutions on 7H10 agar.

3.3.9 Outgrowth assay

M. tuberculosis was grown to mid-log phase in 7H9 media. Bacteria were diluted to OD_{600} nm 0.1 in 200 µL and cultured in 96 well plates with specified media at pH 4.5 or 6.5. H_2O_2 was added to bacterial cultures at specified concentrations. Bacteria were incubated with stressors for 72 hours, after which bacteria were pelleted by centrifugation and washed with PBS. Following washing, PBS was removed and standard 7H9 was used to re-suspend the bacteria. Bacterial OD_{600} nm measurements were taken immediately and every 24 hours thereafter to assess viability. Final OD_{600} nm measurements are reported after normalization to appropriate control that was not exposed to H_2O_2.

3.3.10 Measurement of redox homeostasis

M. tuberculosis strains were transformed with a plasmid expressing mrx1-roGFP2 and grown to mid-log phase in 7H9. Bacteria were diluted to OD_{600} nm 0.25 in 200 µL of specified media and added to 96 well plates. Upon addition of H_2O_2, fluorescent emissions were read at 510 nm after excitation at 390 nm and 490 nm. Values reported are emissions ratios of values detected following excitation at 390 nm relative to 490 nm and were measured 20 minutes following addition of H_2O_2.

3.3.11 *Measurement of lipid peroxide accumulation*

M. tuberculosis strains were grown to mid-log phase in standard 7H9. Bacteria were diluted to OD_{600} nm 0.25 in 10 mL standard 7H9 media at pH 4.5 and labeled with 0.5 uM BODIPY 581/591 C11 (D3861; ThermoFisher Scientific) for 2 hours. Following labeling, 5 mM H_2O_2 was added and 200 µL of bacteria were added to a black 96 well plate. Fluorescent emissions were read at 635 nm and 535 nm following excitation at 590 nm and 485 nm, respectively. Reported values are a ratio of 535 nm emission intensities relative to sum of total emission intensities as suggested by (et al.).

3.3.12 Mouse cell culture

Macrophages were derived from bone marrow of C57BL/6 mice by flushing cells from femurs and culturing in DMEM with 10% FBS and 10% supernatant from 3T3-M-CSF cells for 6 days, with feeding on day 3. After differentiation, BMDMs continued to be cultured in BMDM media containing M-CSF.

3.3.13 M. tuberculosis in vitro infections

BMDMs were seeded at a density of 5e4 cells per well in a 96-well dish seeded at a density of 2.5e5 and 5e4 cells per well, respectively. BMDMs were allowed

to adhere overnight and then infected with DMEM supplemented with 5% FBS and 5% horse serum (BMDMs) at the multiplicities of infections specified. Following a 4-hour phagocytosis period, infection media was removed and cells were washed with room temperature PBS before fresh, complete media was added. For CFU enumeration, media was removed and cells were lysed in water with 0.5% Triton-X and incubated at 37C for 10 minutes. Following the incubation, lysed cells were re-suspended and diluted serially in PBS with 0.05% Tween-80. Dilutions were plated on 7H10 plates.

3.3.14 Transposon-sequencing screen

A transposon mutant library in H37Rv was grown to mid-log phase in 7H9. Bacteria were diluted to and OD of 0.1 in 10 mL 7H9 at pH 4.5 with 2.5 mM H_2O_2. Mutants were exposed to these stressors for 72 hours and then diluted to 15,000 CFU/mL in PBS with 0.05% Tween-80. Approximately 30 thousand bacteria were plated onto six 245 mm x 245 mm 7H10 plates supplemented with 0.05% Tween-80 and Kanamycin (50 ug/mL). Control libraries were not exposed to pH or H_2O_2 and were plated onto 7H10 plates. Colonies grew for 21 days and gDNA preparation and Tn-seq analysis were performed as outlined in the previous chapter.

3.4 Results

3.4.1 Mycobacterium tuberculosis endogenously produces nanocompartments containing DypB cargo proteins

To determine if *Mycobacterium tuberculosis* produces assembled nanocompartments, wild type H37Rv cultures were grown to mid log-phase in axenic culture and lysed. Bacterial supernatants were pelleted through sucrose cushions and further purified by 10-50% sucrose gradient centrifugation. Collected fractions were analyzed by SDS-PAGE. Previous studies in other bacterial species have shown that purified, assembled nanocompartments are distinguishable by their very high molecular weight (Cassidy-Amstutz et al., 2016). Indeed, a band greater than 260 kDa was observable in sucrose fractions ran on SDS-PAGE gels (Fig. 1A). Boiling the sample resulted in disassembly of the high molecular weight complex into protein subunits corresponding to a band approximately 29 kDa, which is the size of the encapsulin shell protein monomer, Cfp29 (Fig. 1A). Transmission electron microscopy of fractions containing possible nanocompartments revealed *M. tuberculosis* produces a structure bearing similarities to previously identified nanocompartments (Fig. 1B). The putative nanocompartments measured 25 nm in diameter and had the characteristic icosahedral shape of bona fide nanocompartments (Sutter et al., 2008; Contreras et al., 2014; Cassidy-Amstutz et al., 2016). To confirm the identity of the nanocompartment shell and identify cargo proteins packaged within, mass spectrometry analysis of the large protein complex was performed.

Results from mass spectrometry identified four proteins: Rv0798c (Cfp29), Rv0799c (DypB), Rv1762c, and Rv2441c (Table 1). The gene Rv2441c encodes a ribosomal protein not reproducibly identified in later preparations and was likely a contaminant. Rv1762c is an unknown protein previously identified in cell membrane fractions but was reproducibly found in purified nanocompartments. FolB and BrfB, which were identified as cargo proteins by Contreras et al. were not found in nanocompartment preparations from *M. tuberculosis*.

3.4.2 Nanocompartments are essential for combatting oxidative and acid mediated stress and for maintaining redox homeostasis

Mycobacterium tuberculosis has genes that encode for 15 putative peroxidases, but only one dye-decoloring peroxidase. Interestingly, type B dye-decoloring peroxidases found in other bacterial species have the highest enzymatic activity at acidic pH levels (Sugano et al. 200, Uchida et al., 2015). To validate the function of the *M. tuberculosis* encoded DypB and find the pH optimum, we heterologously expressed a SUMO-tagged DypB construct in *E. coli* and purified the enzyme. Next, we tested the peroxidase activity over a range of pH levels by performing an ABTS assay, which revealed DypB has maximal activity at pH 4.5 (Fig. 2A). These data suggest that DypB might be most relevant for protection under acidic conditions. We next addressed whether the *M. tuberculosis* encapsulin system confers protection to bacteria in response to oxidative or pH stress. To test this, *M. tuberculosis* mutants with a transposon inserted in *dypb* (Tn::DypB) were cultured in 7H9 media with 2.5 mM H_2O_2 with and without acid stress. Tn::DypB mutants were not susceptible to H_2O_2 mediated stress in broth at neutral pH levels, nor were they more susceptible to acid stress. However, DypB mutants were remarkably susceptible to H_2O_2 in acidified broth (pH 4.5) and displayed 4 logs of attenuation within 24 hours (Fig. 2B). To test if protection of *M. tuberculosis* against a combination of acid and oxidative stress was conserved across most *M. tuberculosis* peroxidases, we performed a transposon-sequencing screen. A library of *M. tuberculosis* transposon mutants was exposed to H_2O_2 and acid stress for 72 hours. Surviving mutants were analyzed using Illumina sequencing. Analysis of the results revealed DypB and KatG (catalase-peroxidase) were the only two enzymes with annotated peroxidase function that were essential for survival of *M. tuberculosis* in these restrictive conditions (Table 2). This suggests nanocompartments perform a rare function in protecting *M. tuberculosis* from oxidative and pH stress.

Inadequate response to ROS can result in disruption of oxidation-reduction homeostasis and bacterial death. Since DypB functions as a peroxidase that can detoxify H_2O_2, we tested whether attenuation of Tn::DypB mutants correlated with altered redox homeostasis in the bacteria. To determine this, we added a reporter plasmid expressing a mycoredoxin and reduction-oxidation sensitive GFP fusion protein (mrx1-roGFP) to the bacteria. Mycothiol, similar to

glutathione, is the main antioxidant in the bacterial cytosol as it provides a reducing substrate to protect *M. tuberculosis* from oxidative stress. Mycoredoxin is a mycothiol-specific oxidoreductase and is harnessed in this system to measure changes in the redox state of mycothiol. Upon exposure to ROS, oxidation of mycothiol is reflected by subsequent oxidation of two free cysteine residues in roGFP. Formation of the disulfide bond in roGFP causes an increased shift in the fluorescent intensity measured at 390 nm and concomitant decreased fluorescent intensity at 490 nm. The reaction is reversible: reduction of the disulfide bond reverses the change in fluorescent intensities, which allows for real-time measurement of redox states in the bacteria. Nanocompartment mutants (ΔOperon) had higher fluorescent emission ratios at baseline measurements, independent of pH, indicating the cytosol was more oxidized than wild-type bacteria (Fig. 2C). Addition of H_2O_2 increased levels of oxidation in both wild-type and mutant bacteria, although nanocompartment mutants still had higher oxidation levels. These data show nanocompartments are important for maintaining redox homeostasis, even in a non-hostile environment.

3.4.3 Encapsulation of DypB is necessary for full protection of M. tuberculosis against oxidative and acid stress

While the transposon mutant used in these studies has an insertion in *dypb*, we discovered Tn::DypB mutants do not assemble functional nanocompartment structures (Fig. 3A, not shown). Therefore, we generated constructs to complement the mutant with plasmids expressing DypB, Cfp29, or the whole operon (Fig. 3B). Complementation of Tn::DypB with the peroxidase (Tn::DypB + pDypB) partially rescued bacterial growth when exposed to 2.5 mM H_2O_2 at pH 4.5 (Fig. 3C). However, complementation with the nanocompartment operon (Tn::DypB + pOperon) completely rescued growth of Tn::DypB mutants under these conditions (Fig. 3C). The degree of rescue mediated by the unpackaged enzyme was surprising as it is hypothesized the nanocompartment shell protects cargo proteins and may facilitate the peroxidase reaction. However, complementation was performed using anhydrotetracycline overexpression vectors, so it is possible that overexpression of DypB compensated for the enzyme being unpackaged. Complementation of Tn::DypB mutants with just the encapsulin shell protein (Tn::DypB + pCfp29) provided no additional protection from H_2O_2 and acid stress (Fig. 3C). While these data suggested that encapsulation of the peroxidase is essential for complete survival of *M. tuberculosis* under these conditions, we sought to confirm this by testing the susceptibility of different knockouts to oxidative and acid stress. Knockouts lacking the encapsulin shell (ΔCfp29), the peroxidase (ΔDypB), or the whole nanocompartment (ΔOperon) were generated in H37Rv *M. tuberculosis*. Importantly, ΔDypB mutants, like Tn::DypB mutants, failed to assemble a nanocompartment shell. Following 24 hour exposure to H_2O_2 and acid stress, ΔOperon and ΔDypB mutants were attenuated by 2.5 and 2 logs, respectively (Fig. 3D). After three days of exposure, ΔCfp29 mutants were also significantly

attenuated by half a log, in comparison to wild type *M. tuberculosis* (Fig. 3D). Together, these data confirm DypB activity is required for survival of *M. tuberculosis* under conditions of oxidative and pH stress and is further enhanced by encapsulation.

3.4.4 Susceptibility of nanocompartment mutants to oxidative and acid stress is mediated by free fatty acids

It was intriguing that nanocompartment mutants were only hypersusceptible to a combination of oxidative stress and acidified media. While our analysis revealed DypB peroxidases have the highest enzymatic activity at pH 4.5 and are essential for growth under those conditions, we speculated that acidification of the media was generating toxic free fatty acid byproducts, to which *M. tuberculosis* is very sensitive (Dubos, 1947; Vandal et al., 2008). *M. tuberculosis* is cultured in 7H9, a complete and chemically defined media that is supplemented with glycerol, albumin-dextrose-saline, and Tween-80. Tween-80 is a surfactant that reduces bacterial clumping, but under acidic conditions it can be hydrolyzed to oleic acid, which can potentially permeabilize the bacterial membrane (Vandal et al., 2008). Additionally, Tween-80 can remove the *M. tuberculosis* glycoprotein capsule, which may also enhance susceptibility to acid stress (Ortalo-Magne et al.,1996). To determine if Tween-80 was contributing to attenuation of nanocompartment mutants, Tween-80 was replaced with a nonhydrolyzable surfactant, Tyloxapol. While Tyloxapol may still disrupt the bacterial capsule, it does not generate oleic acid. When we performed acid and H_2O_2 susceptibility tests in media supplemented with Tyloxapol, nanocompartment mutants were attenuated by almost 4 logs after 24 hours of exposure (Fig. 4A). We next tested the susceptibility of nanocompartment mutants to the stressors in Sauton's minimal media, another chemically defined media that was supplemented with glycerol and Tyloxapol. Intriguingly, nanocompartment mutants were not susceptible to oxidative and acid stress in the minimal media (Fig. 4B). One of the major differences between 7H9 and Sauton's minimal media is the use of albumin as a carbon source. 7H9 media is supplemented with 10% albumin-dextrose-saline, and most preparations of albumin have an abundance of associated fatty acids (Curry et al., 1999, Van Der Vusse, 2009). We hypothesized that acidification of 7H9 liberated fatty acids associated with albumin and that free fatty acids were mediating toxicity. To test this, 7H9 was prepared with standard BSA and fatty acid free BSA. Culturing nanocompartment mutants in fatty acid free media was sufficient to reverse the phenotype and bacteria survived exposure to 1.3 mM H_2O_2 at pH 4.5, even after 72 hours (Fig. 4C). These data confirmed that free fatty acids generated from media acidification were mediating toxicity to nanocompartment mutants when exposed to oxidative stress, but not wild-type *M. tuberculosis*.

3.4.5 Possible mechanisms of fatty acid mediated toxicity

There were two major hypotheses as to why free fatty acids were toxic to nanocompartment mutants. First, free fatty acids may disrupt the cell membrane of *M. tuberculosis* and lead to acidification of the bacterial cytosol and enhance susceptibility to H_2O_2 (Ibarguren et al., 2014). We previously demonstrated nanocompartments package a peroxidase that is optimally active in acidic environments (Fig. 2A), and is rare in its ability to confer protection to bacteria when exposed to a combination of acid and oxidative damage (Table 2). Therefore, any membrane damage would likely be lethal to mutants lacking a functional nanocompartment system. Another possibility is that acidification of the media and addition of H_2O_2 may produce reactive lipid peroxides. Hydrogen peroxide can be rapidly converted to hydroxyl and hydroperoxyl radicals via the Fenton reaction. The free radicals react with unsaturated lipids to produce lipid radicals, which self-propagate and eventually terminate with the generation of highly reactive aldehydes (Yin et al., 2011). Like free fatty acids, lipid peroxides and reactive aldehydes may disrupt the cell membrane of *M. tuberculosis* and lead to cytosol acidification, but they may play another role as well (Girotti, 1998). Certain peroxidases detoxify lipid peroxides by converting them into stable lipid alcohols. In this scenario, DypB may catalyze lipid peroxide reduction while oxidizing an unknown substrate. If nanocompartments are important for detoxifying lipid peroxides, mutants should have increased accumulation of lipid peroxides. To test the latter theory, we labeled *M. tuberculosis* with Bodipy 581/591 undecanoic acid C11, a lipid peroxidation sensor. Bodipy C11 has a polyunsaturated butadienyl region that is oxidized by lipid peroxides. Upon oxidation, the probe's fluorescent emission peaks shifts from red (~590 nm) to green (~510 nm). Following Bodipy C11 labeling, bacteria were exposed to 5 mM H_2O_2 at pH 4.5, and fluorometric measurements were taken. While addition of H_2O_2 did increase lipid peroxide levels, there were no discernable differences between wild-type and ΔOperon mutants (Fig. 5). These data suggest that free fatty acids from acidified media are not causing excessive accumulation of lipid peroxides in the nanocompartment mutant. However, we have yet to determine if the cell membrane is being damaged by free fatty acids, lipid peroxides, or otherwise.

3.4.6 Bacterial nanocompartments are required for full virulence during macrophage infection

Nanocompartment mutants were significantly attenuated when exposed to ROS and acid, two stressors that are found in phagolysosomes. Interestingly, a transposon-sequencing screen performed by our lab identified the Cfp29 gene as essential for survival of *M. tuberculosis* in human macrophages activated with IFN-γ (Fig. 6A). To validate attenuation of nanocompartment mutants, we infected mouse bone marrow-derived macrophages with wild-type and mutant bacteria, and enumerated CFU. Tn::DypB, ΔCfp29, and ΔOperon mutants were

significantly attenuated for growth in macrophages over 3- or 4-day time-courses. Thus, nanocompartments not only play an integral role in protecting *M. tuberculosis* from artificially generated stressors, but are essential for complete virulence in the harsh environment of a phagolysosome as well.

3.5 Discussion

Nanocompartments are proteinaceous organelles that are broadly conserved across bacteria and archea (Giessen and Silver, 2017). In this work, we show *M. tuberculosis* endogenously produces nanocompartments that are 25 nm in diameter. Our analysis revealed the encapsulin protein, Cfp29, forms the hollow shell of the nanocompartment and dye-decoloring peroxidases (DypB) are packaged inside. Interestingly, all nanocompartment purifications identified an unknown protein (Rv1762c) as being associated with the nanocompartment. While the function of this protein remains unknown, it is worth studying to see if this protein may facilitate nanocompartment assembly or substrate delivery. A previous study reported that *M. tuberculosis* packages three cargo proteins: DypB, BfrB, and FolB (Contreras et al., 2014). However, this study was performed by heterologous over-expression of a single cargo protein in conjunction with the encapsulin shell in *E. coli*. Other studies that analyzed mechanisms of cargo packaging in nanocompartments showed cargo loading is dependent on protein abundance and the presence of other competing cargo proteins (Giessen et al., 2017; Cassidy-Amstutz et al; 2016). Thus, heterologous over-expression may falsely identify proteins that are not packaged endogenously.

While *M. tuberculosis* has genes encoding for a variety of other putative peroxidases, there is only one dye-decoloring peroxidase. DypB belongs to a family of heme-peroxidases that are noted for their ability to degrade phenolic dyes and some have enhanced enzymatic activity at acidic pH levels (Chen and Li, 2016). Results from our study and others confirm the function of DypB as a peroxidase, and here we show the enzyme is optimally active at pH 4.5 (Contreras et al., 2014). Interestingly, we found that nanocompartment mutants lacking the shell and peroxidase are hypersusceptible to a combination of oxidative and acid stress, but not to either of the stressors independently.

The ability to confer protection against oxidative and pH stress is not conserved amongst the other putative peroxidases encoded by *M. tuberculosis*. Data from our transposon-sequencing screen identified DypB and KatG (catalase-peroxidase) as the only two annotated peroxidase genes essential for survival against these stressors, which has intriguing implications. Isoniazid, a first-line antibiotic used to treat tuberculosis infections, is a pro-drug that inhibits fatty acid synthases (Timmins and Deretic, 2006). Isoniazid is activated by KatG and mutations in KatG can arise over the course of exposure to isoniazid, usually as a result of improper antibiotic administration. Approximately 15% of clinically

isolated *M. tuberculosis* strains have isoniazid resistance, which shows the remarkable prevalence and viability of this drug-resistant strain (Jenkins et al., 2011). In KatG mutants, a suppressor mutation is frequently found in the transcriptional regulator region for a gene encoding ahpC, an alkyl hydroperoxidase, which results in over-expression of ahpC (Sherman et al., 1996; Wilson et al., 1999; Baker et al., 2005; Dalla Costa et al., 2009). There are several studies that suggest ahpC over-expression helps compensate for the loss or reduction of KatG function by detoxifying ROS and RNI (Chen et al, 1998; Nathan and Shiloh; 2000). Our Tn-seq results show transposon mutants with an insertion in ahpC were slightly attenuated in response to acid and oxidative damage, but the results were not statistically significant. This implies ahpC is dispensable under those conditions tested. Most enzymes are not active at acidic pH, so if the membrane of *M. tuberculosis* is damaged by stressors in the phagolysosome or by antibiotics, acidification of the bacterial cytosol likely inactivates other peroxidases. In contrast, the *M. tuberculosis* bacterial nanocompartment is exquisitely suited to detoxify H_2O_2 in the presence of acid stress and could help confer protection to KatG mutants in addition to wild-type bacteria. Further testing of the relationship between nanocompartments and KatG will be performed by making a triple knockout in KatG, DypB and Cfp29 and measuring bacterial attenuation. The results of this study could importantly reflect upon the prevalence of clinically isolated isoniazid-resistant mutants and identify nanocompartments as a potential drug target to treat isoniazid-resistant *M. tuberculosis.*

Hypersusceptibility of nanocompartment mutants to H_2O_2 and acid was dependent on the presence of free fatty acids in the media. While the mechanism by which free fatty acids mediate toxicity remains unclear, our main hypothesis is that free fatty acids, or potentially lipid peroxides, are disrupting the membrane of *M. tuberculosis* resulting in acidification of the bacterial cytosol. Acidification of the bacterial cytosol will be examined using a pH-sensitive GFP reporter. If free fatty acid mediated toxicity is indeed due to membrane perturbation and disruption of intracellular pH, then other mechanisms that cause perturbations of pH homeostasis should attenuate nanocompartment mutant bacteria as well. Pyrazinamide is another first-line antibiotic used to treat tuberculosis. It is a pro-drug that is activated by acidic pH (~5) and has reduced the antibiotic treatment regimen from 9 to 6 months, demonstrating its potent efficacy in humans (Zhang et al., 2003; Via et al., 2015). Pyrazinamide disrupts the membrane of *M. tuberculosis* resulting in acidification of the bacterial cytosol and death. (Zhang et al., 1999; Zhang et al., 2003). Thus, it is thought that pyrazinamide works in conjunction with the acidic phagolysosome environment, which delivers ROS and RNI, to restrict *M. tuberculosis* growth. Since nanocompartment mutants are hypersusceptible to the same stressors that pyrazinamide exploits, we will test if nanocompartment mutants are more sensitive to pyrazinamide. If so, this will further justify drug development to target nanocompartment function.

In addition to showing nanocompartment mutants are essential for survival when exposed to oxidative and pH stress *in vitro*, we discovered that nanocompartment mutants are attenuated for survival in mouse macrophages. This supports the hypothesis that nanocompartments play an essential role for survival in the phagolysosome where bacteria form a replicative niche and are exposed to similar stressors. To consolidate what we discovered about *M. tuberculosis* nanocompartments in this study and what we knew from prior research, we propose the following model (Figure 7). Following phagocytosis, lysosomes fuse with phagosomes to form the phagolysosome. Vacuolar ATPases that pump protons across membranes are now associated with the phagolysosome complex and acidify the vesicle to pH ~5 (Xu and Ren, 2015). Additionally, lysosomes deliver a variety of antimicrobial peptides and acid activated hydrolytic enzymes that facilitate break down of proteins, carbohydrates, lipids, and nucleic acids (Xu and Ren, 2015). Upon activation of macrophages, there is enhanced assembly of the NADPH oxidase on the membrane of phagolysosomes, which generates superoxide and other reactive oxygen species (Bedard and Krause, 2007). While it has been shown that some *M. tuberculosis* bacteria can survive in the harsh phagolysosome environment, a portion of bacteria lyse and release their cytosolic contents into the phagosome (Vandal et al., 2008). Studies of nanocompartments in *T. maritima* have shown the nanocompartment shell is resistant to acid denaturation and proteases, so exposed nanocompartments may persist in the phagolysosome and carry out detoxification of H_2O_2 to protect surviving bacteria (Cassidy-Amstutz et al, 2016). Additionally, there are still nanocompartments in the living bacteria that may protect *M. tuberculosis* in the event of membrane perturbation, thus providing a role for nanocompartments intracellularly and extracellularly.

Other proteins in *M. tuberculosis* have been shown to protect the bacteria from a combination of acid and oxidative stress, which are two main features of the phagolysosome environment (Vandal et al., 2009). In fact, one membrane serine protease that is essential for bacterial survival in acidic environments is preferentially activated upon oxidation (Biswas et al., 2010). This suggests there is a subset of proteins that are optimally active in the phagolysosome when other proteins are rendered incapable by low pH and oxidative damage and nanocompartments are a part of them. While more research is necessary to validate our proposed model, our study provides one of the best characterizations of the physiological role of nanocompartments and valuable insight on how *M. tuberculosis* survives within the macrophage.

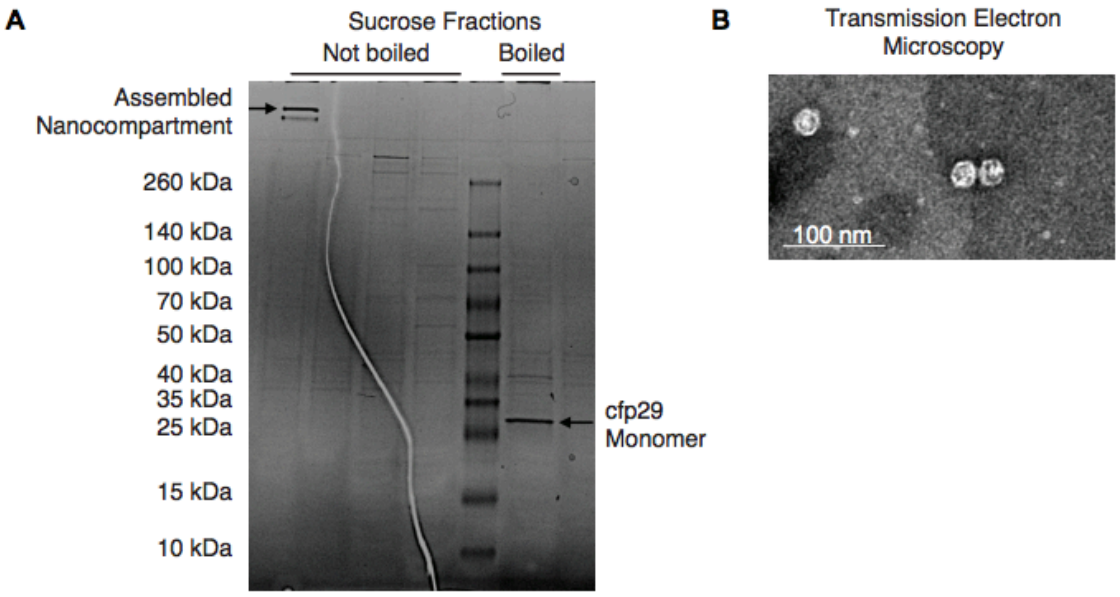

Figure 1. Purification of endogenous nanocompartments from *M. tuberculosis.* **A.** Coomassie stained SDS-PAGE of not boiled (left) or boiled (right) sucrose fractions depicting encapsulin shell protein, Cfp29. Lysates were prepared from wild-type H37Rv *M. tuberculosis*. B. Negative stained transmission electron microscopy of purified Cfp29 encapsulin shell proteins

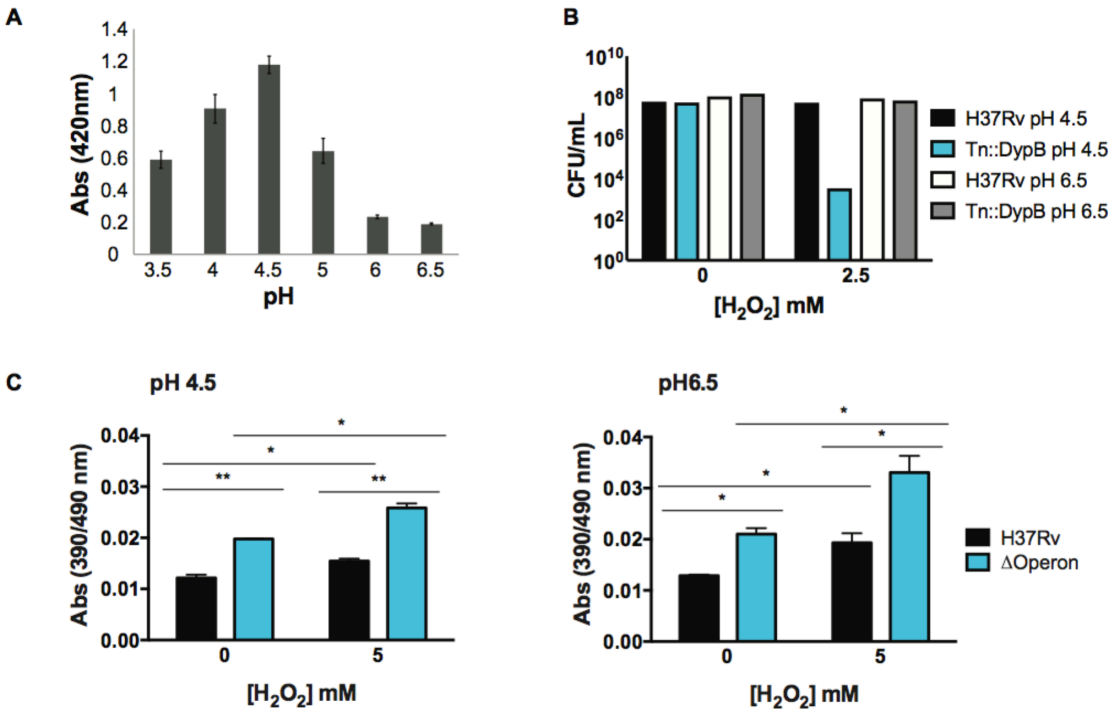

Figure 2. DypB is a peroxidase essential for protection against oxidative and acid stress and maintenance of redox homeostasis. **A.** Apo-SUMO-DypB (538 nM) peroxidase activity using ABTS (480 nM) as a substrate in the presence of H_2O_2 (480 nM) at varying pH levels was monitored by observing the change in absorbance at 420 nm after 20 minutes. **B.** Wild type and mutants with a transposon inserted in DypB (Tn::DypB) were exposed to combinations of oxidative (2.5 mM H_2O_2) and acid (pH 4.5) stress for 24 hours before assessing bacteria viability by plating for CFU. **C.** Wild-type and nanocompartment mutant bacteria lacking the operon Rv0798c-99c (ΔOperon) were transformed with a reporter plasmid expressing mycoredoxin fused to a reduction-oxidation sensitive GFP. Upon exposure to a combination of oxidative (5 mM H2O2) and acid (pH 4.5) stress for 20 minutes, the redox state of bacteria were assessed by measuring the shift in fluorescence emissions from 490 nm to 390 nm. Values reported as a ratio to control for differences in plasmid expression. **A** and **C** are representative of two independent experiments. **B** is representative of over 3 independent experiments. The p values were determined using an unpaired t test. *$p<0.05$, **$p<0.01$.

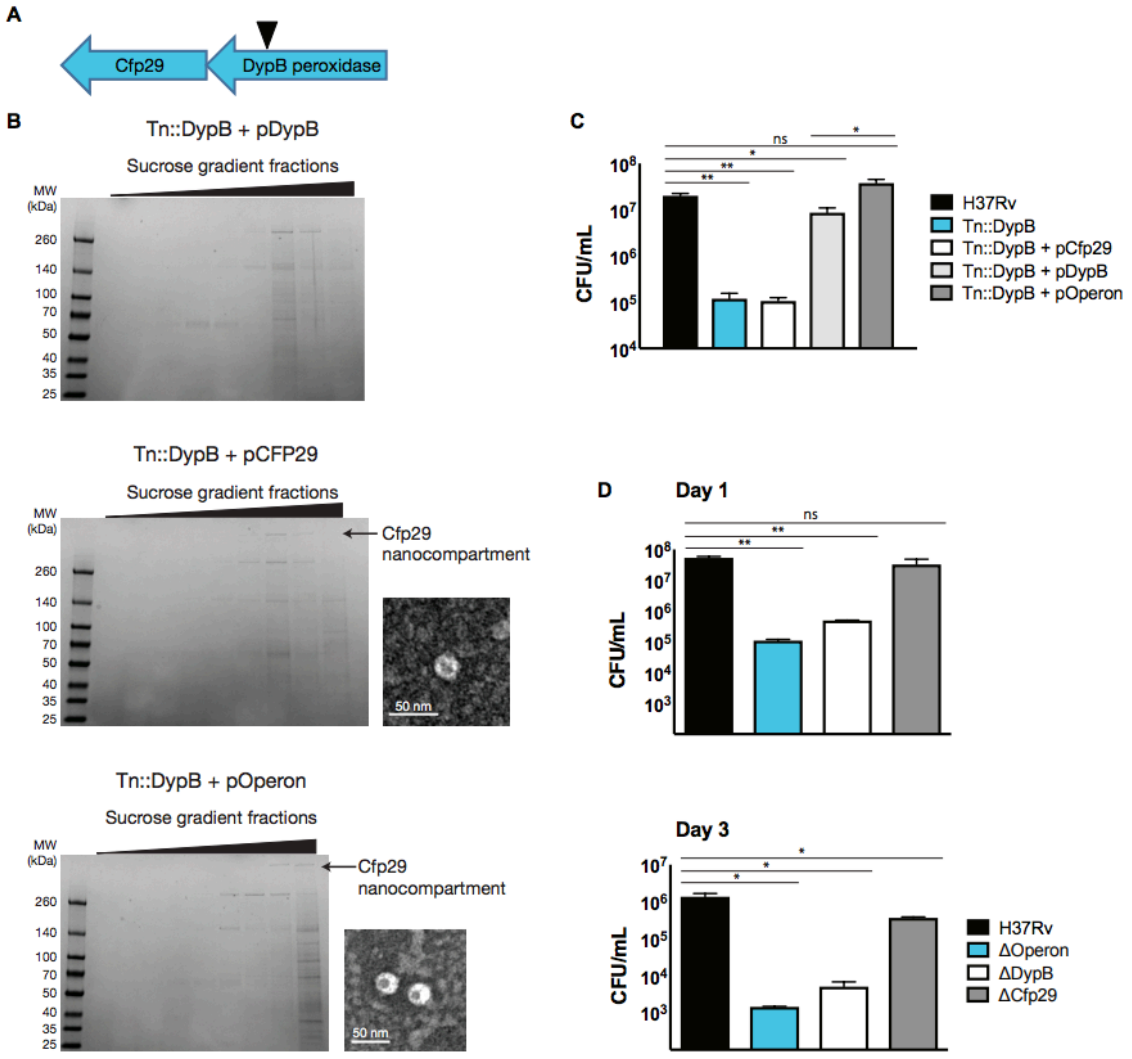

Figure 3. Encapsulation of DypB is required for optimal growth of *M. tuberculosis* in the presence of oxidative and acid stress. **A**. Schematic of the nanocompartment operon depicting the transposon insertion site in DypB. **B.** Coomassie stained SDS-PAGE of sucrose fractions showing encapsulin shell protein, Cfp29 and corresponding transmission electron microscopy of purified Cfp29. Lysates were prepared from Tn::DypB *M. tuberculosis* mutants complemented with DypB (upper), Cfp29 (middle), and nanocompartment operon (lower). **C.** Wild type bacteria, Tn::DypB mutants, and mutants complemented with ATc (200 ng/mL) inducible over-expression plasmids expressing the peroxidase (pDypB), the encapsulin shell (pCfp29) and nanocompartment operon (pOperon) were exposed to oxidative (2.5 mM H_2O_2) and acid (pH 4.5) stress for 24 hours before assessing bacteria viability by plating for CFU. D. Wild type bacteria and knockout mutants lacking the peroxidase (ΔDypB), the encapsulin shell (ΔCfp29) and the whole nanocompartment operon (ΔOperon) were exposed to oxidative (2.5 mM H_2O_2) and acid (pH 4.5) stress for 24 (upper) and 72 (lower) hours before assessing bacteria viability by plating for CFU. Note: ΔDypB functionally lacks Cfp29 and doesn't assemble a nanocompartment. **C** and **D** are representative of 2 experiments. The p values were determined using an unpaired t test. *p<0.05, **p<0.01, ns: not significant.

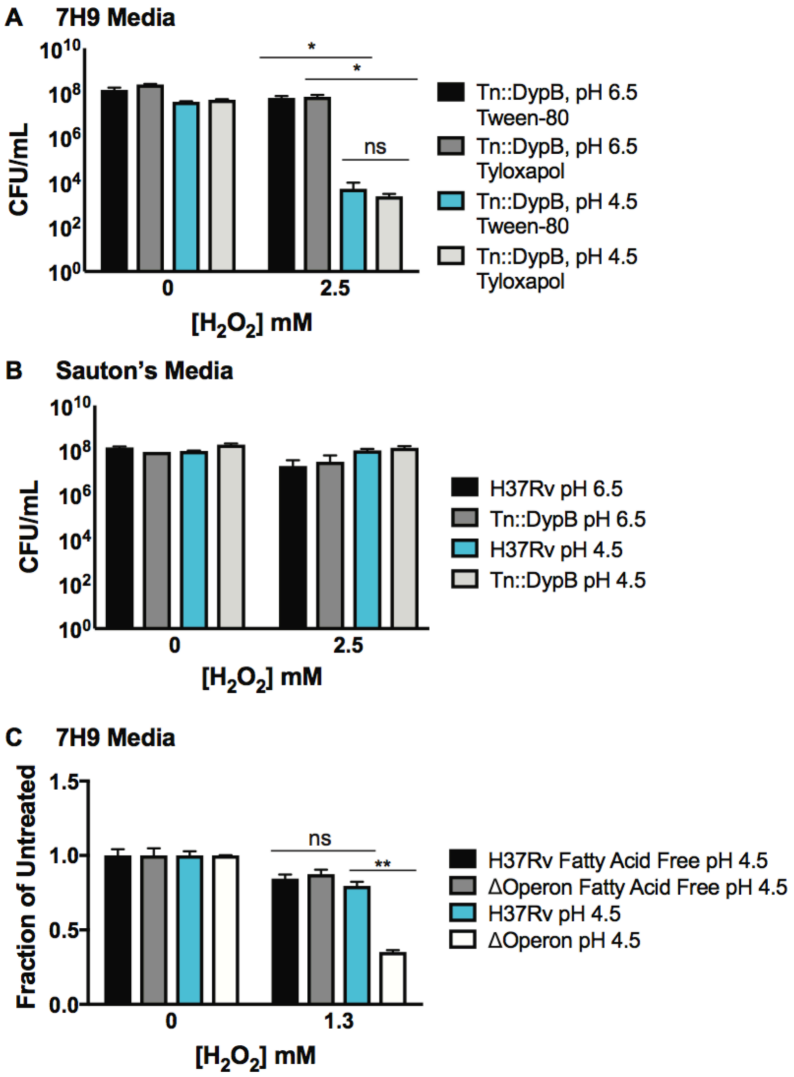

Figure 4. Hypersusceptibility of nanocompartment mutants to acid and oxidative stress is mediated by presence of free fatty acids. Wild type *M. tuberculosis* and mutants with a transposon inserted in DypB (Tn::DypB) were exposed to combinations of oxidative (2.5 mM H_2O_2) and acid (pH 4.5) stress for 24 hours in the following medias for 24 hours before plating for CFU: **A.** 7H9 media supplemented with glycerol, albumin and either Tween-80 or Tyloxapol and **B.** Sauton's minimal media supplemented with glycerol and Tyloxapol. **C.** Wild type and mutants lacking the nanocompartment operon (ΔOperon) were exposed to combinations of oxidative (1.3 mM H_2O_2) and acid (pH 4.5) stress for 72 hours in 7H9 media supplemented with glycerol, Tyloxapol, and either fatty-acid free BSA or standard BSA preparations. Following exposure an outgrowth assay was performed. OD_{600} nm measurements were taken daily. OD_{600} nm values are normalized to bacteria exposed to acid stress but not oxidative stress during the first 72 hours. **A-C** are representative of two or more experiments. The p values were determined using an unpaired t test. *$p<0.05$, **$p<0.01$, ns: not significant.

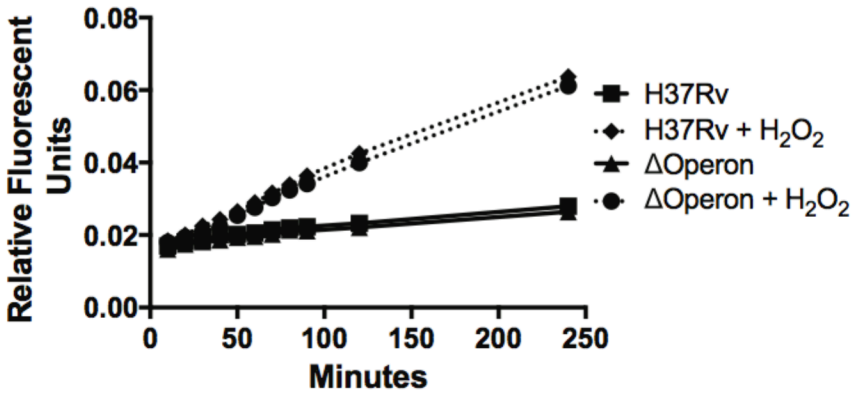

Figure 5. Nanocompartment mutants do not accumulate excess lipid peroxides. Wild type *M. tuberculosis* and mutants with deletions of the nanocompartment operon (ΔOperon) were labeled with Bodipy 581/591 undecanoic acid C11 (0.5 uM) in acidified media (pH 4.5) for 2 hours. Following labeling, bacteria were exposed to oxidative stress (5 mM H_2O_2) and oxidation of the probe was measured by a shift in the fluorescent emission peak from 635 nm to 535 nm. Absorbance is reported as relative fluorescent units (535 nm intensity normalized to the total intensity). Data are representative of two experiments.

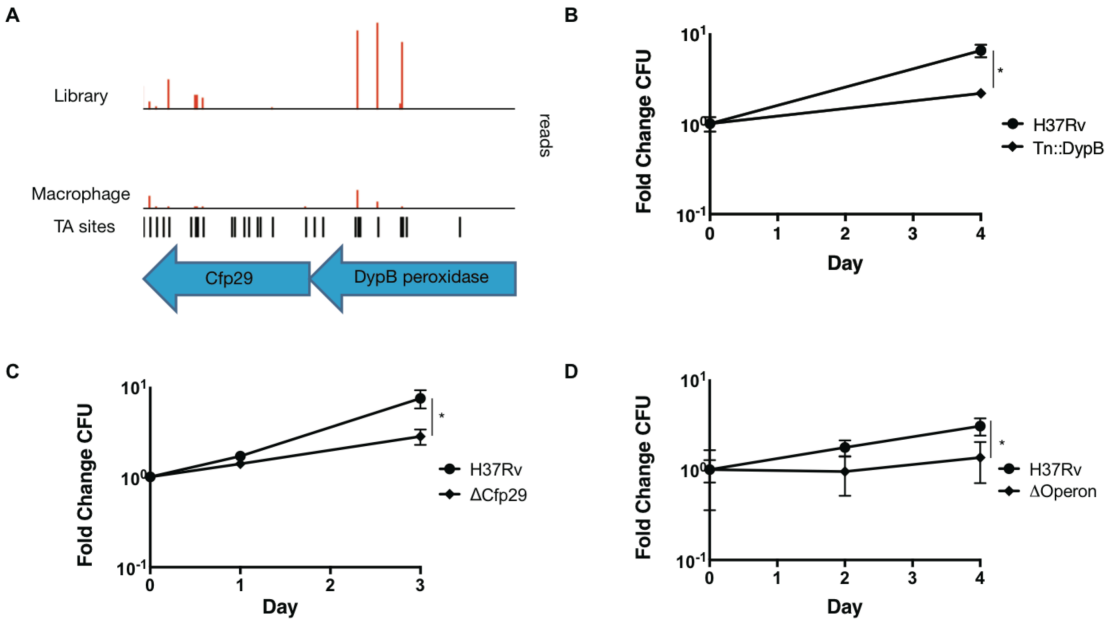

Figure 6. Nanocompartment mutants are attenuated for survival in macrophages. **A.** Transposon insertion density map for the nanocompartment operon displaying the number of sequencing reads (red) mapped to genes in the control library and mutants that were passaged through human macrophages activated with IFN-γ. Black bars denote all possible transposon insertion sites; Red bars denote actual insertion sites. Mouse bone marrow-derived macrophages infected with wild-type *M. tuberculosis* or mutants with a (**B**) transposon inserted in DypB (Tn::DypB) (**C**) deletion of the encapsulin shell protein (ΔCfp29) or (**D**) deletion of the whole nanocompartment operon (ΔOperon). Macrophages were infected with MOI of 1 (**B** and **D**) or MOI 5 (**C**) and CFU were enumerated immediately following phagocytosis and at days 2 and 4 or 1 and 3, respectively. Error bars are SD from 4 replicate wells. Data shown are representative of 3 experiments (**B)** and from 1(**C** and **D**) experiments. The p values were determined using an unpaired t test, *p≤0.05.

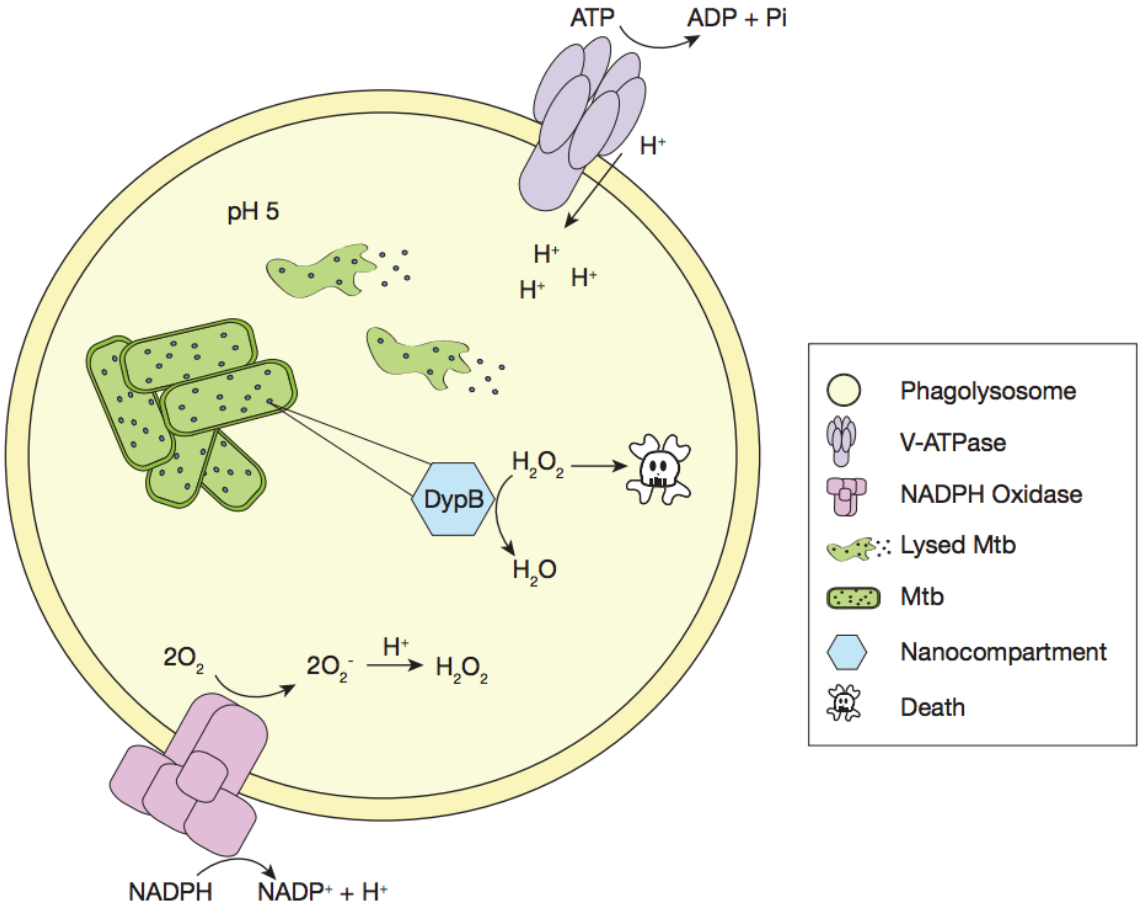

Figure 7. Nanocompartments are essential for survival of *M. tuberculosis* in the harsh environment of the phagolysosome. In the phagolysosome environment, bacteria are exposed to oxidative damage via the NADPH oxidase and acid stress from fusion with lysosomes that contain vacuolar ATPases and pump protons into the vesicle. Nanocompartments are stable and contain a peroxidase that is preferentially activated in these conditions and may function inside the bacteria or extracellularly to detoxify H_2O_2.

Table 1: Peptide counts from mass spectrometry analysis of nanocompartments purified from H37Rv *M. tuberculosis*

Gene	**Protein**	**Counts**
Rv0798c	Cfp29	1298
Rv0799c	DypB	343
Rv1762c	Unknown	113
Rv2441c	RpmA	6

Table 2: Essentiality predictions for enzymes annotated as peroxidases, catalases and superoxide dismutases following exposure to acid and oxidative stress

Gene	Description	log2 FC	p-value	p-adj	Prediction
Rv1908c	catalase-peroxidase-peroxynitritase T KatG	-6.95	0.00	0.00	Essential
Rv0799c	dyp-type peroxidase	-3.07	0.00	0.26	Essential
Rv2159c	alkylhydroperoxidase AhpD family core domain-containing protein	0.11	0.75	1.00	Not Essential
Rv0464c	alkylhydroperoxidase AhpD family core domain-containing protein	-0.34	0.38	1.00	Not Essential
Rv3473c	peroxidase BpoA	0.67	0.56	1.00	Not Essential
Rv0432	periplasmic superoxide dismutase [Cu-Zn] SodC	-0.03	0.96	1.00	Not Essential
Rv1900c	lignin peroxidase LipJ	0.28	0.58	1.00	Not Essential
Rv1932	thiol peroxidase Tpx	-0.16	0.75	1.00	Not Essential
Rv3177	peroxidase	-0.37	0.58	1.00	Not Essential
Rv1767	alkylhydroperoxidase AhpD family core domain-containing protein	-0.83	0.28	1.00	Not Essential
Rv1123c	peroxidase BpoB	-0.28	0.57	1.00	Not Essential
Rv3171c	non-heme haloperoxidase Hpx	0.57	0.23	1.00	Not Essential
Rv2428	alkyl hydroperoxide reductase AhpC	-0.64	0.50	1.00	Not Essential
Rv0554	peroxidase BpoC	1.57	0.00	0.23	Not Essential
Rv2429	alkyl hydroperoxide reductase AhpD	0.18	0.66	1.00	Not Essential
Rv3846	superoxide dismutase [Fe] SodA	0.11	0.88	1.00	Not Essential

Chapter Four

Remaining questions and concluding remarks

4.1 Transposon-sequencing screen in human and mouse macrophages

4.1.1 Summary of results

The first part of this study identified genes essential for *M. tuberculosis* growth in human and mouse macrophages. Further validation of conditionally essential candidates is needed to identify genes that are uniquely required for growth in each condition. However, we show human and mouse macrophage environments are disparate and certain to have repercussions on bacterial fitness and survival. One of the main differences observed was in IFN-γ activation of human and mouse macrophages. IFN-γ activation of mouse macrophages results in robust NO production and restriction of *M. tuberculosis* growth (Chan et al., 1992). In contrast, we show IFN-γ does activate human macrophages, but macrophages do not produce NO, nor do they restrict *M. tuberculosis* growth. Another disparity between the human and mouse macrophage environment is reflected by altered nitrogen metabolism in *M. tuberculosis*. *M. tuberculosis* produces nitrite during infection of human macrophages, but not in mouse macrophages. Traditionally, nitrite production in *M. tuberculosis* is associated with hypoxic conditions and a shift to anaerobic respiration, and other nitrogen metabolites play a role in protecting the bacteria from acid stress (Gouzy et al., 2014). It is uncertain why the bacteria undergo a metabolic shift in human macrophages and if it is important for survival. However, careful analysis of our data set is likely to reveal additional requirements for bacterial growth in human and mouse macrophages that have been previously overlooked.

4.1.2 Remaining questions and future directions

One of the biggest challenges during the transposon-sequencing screen was trying to improve the dynamic range for detection of mutants. *M. tuberculosis* has doubling rate of 18-24 hours in broth and replicates even more slowly in macrophages. Over the course of a four day infection, it is standard to see ~4-fold growth in mouse macrophages and ~7-fold growth in human macrophages. Serially passaging transposon mutants through macrophages significantly increased the number of hits identified and enriched the data set. However, when looking at essentiality classification of genes selected for proof-of-concept validation, the results were mixed. Some mutants known to be attenuated during macrophage infection were not identified in our screen because they did not meet the statistical criteria. In some instances, p values were too high, and in others p values were statistically significant but the mutants did not display more than 2 fold attenuation. Parameters for analysis may be changed so that any attenuated mutant with a significant p value is classified as essential, regardless of fold change in growth. However, this does not solve the problem of mutants with p values on the cusp of statistical significance.

Problems with dynamic range are inherent to every screen involving slow-growing bacteria. To mitigate this, a newer procedure that uses random barcoded transposons and high throughput sequencing (Bar-seq) has been developed (Wetmore et al., 2015). Construction of a barcoded transposon mutant library is similar in theory to construction of a standard transposon library. However, in a standard transposon library, the transposon sequence is identical between mutants. Therefore, it is impossible to determine if reads mapped to one insertion site originate from a single bacterium that replicated or from multiple independent mutants that had insertions at the same site. In barcoded libraries, each transposon has a unique barcode, so mutants with insertions at the same site can be treated as separate events. This has an enormous impact on analysis of the screen as one can achieve statistical significance with a small dynamic range. This technique is a remarkable advancement for slow growing bacteria like *M. tuberculosis* and we are in the process of generating a barcoded library.

The genome of *M. tuberculosis* is not well annotated, which adds an additional layer of complexity to analyzing data from our macrophage screen. Even after mutants have been validated, determining how to characterize a protein annotated as a “conserved hypothetical” is challenging and BLAST results yield mixed returns. One way to broadly annotate gene function is to perform a series of Tn-seq screens where bacteria are exposed to hundreds of experimental conditions, such as acid, oxidative stress, various carbon sources, antibiotics, etc., and look for trends that allude to gene function. However, preparation of samples for traditional Tn-seq screens is laborious, time consuming and very expensive, which renders screening hundreds of conditions unfeasible. To prepare a Tn-seq library for Illumina sequencing, genomic DNA is sheared, purified, end repaired, and polyA-tailed. Following A-tail addition, barcoded adapters are ligated, and transposon-chromosome junctions are amplified by two PCR amplification steps, one of which adds Illumina adapters. As demonstrated by Wetmore et al., Bar-seq streamlines this process. Preparation of samples for Bar-seq entails one step: a PCR to amplify barcodes and simultaneously add Illumina adapters. Once we have created our barcoded transposon mutant library in *M. tuberculosis* we can screen mutants through chemical libraries that will help elucidate gene function.

4.2 Characterization of *M. tuberculosis* nanocompartments

4.2.1 Summary of results

In the second part of this study we perform the first characterization of nanocompartments endogenously produced by *Mycobacterium tuberculosis.* We show that *M. tuberculosis* nanocompartments are comprised of Cfp29 encapsulin shell proteins and dye-decoloring peroxidase (DypB) cargo proteins. The DypB protein functions as a peroxidase that is optimally active at acidic pH

levels. Importantly, we show that nanocompartment mutants are attenuated for survival when exposed to oxidative and acid stress *in vitro*, or in the harsh phagolysosome environment of macrophages. Additionally, we demonstrate that unpackaged DypB peroxidase activity can confer protection to the bacteria when exposed to oxidative and acid stress, but encapsulation of the peroxidase in the nanocompartment shell is necessary for maximal survival. These findings support the hypothesis that nanocompartments, which are known to be acid and protease resistant, function to protect the bacteria from acid and peroxide stress in the phagolysosome when other mechanisms of bacterial defense are rendered inactive. In the event of bacterial lysis, we speculate the nanocompartments persist in the phagolysosome and detoxify H_2O_2 to protect the surviving bacteria.

4.2.2 Remaining questions and future directions

In our study, we showed hyper-susceptibility of nanocompartments mutants to oxidative and acid stress is mediated by free fatty acids. *M. tuberculosis* employs mechanisms to protect the bacteria from acid stress and maintain pH homeostasis in the phagolysosome. Still, it is possible that the combination of excess free fatty acids and oxidative stress permeabilize the membrane of *M. tuberculosis* and disrupt pH homeostasis. To test this we will transform bacteria with a pH-sensitive ratiometric GFP reporter plasmid. This reporter will allow for real-time measurements of the intrabacterial pH of *M. tuberculosis*.

Given the stable nature of previously studied nanocompartments, we speculate *M. tuberculosis* nanocompartments are protease and acid resistant (Cassidy-Amstutz et al., 2016). To test this, we will expose purified nanocompartments to lysosomal proteases, such as Cathepsin B and Cathepsin D, and track the rate of degradation by SDS-PAGE analysis. Similarly, we will track the rate of nanocompartment denaturation in response to acid stress. If nanocompartments are indeed stable, we hypothesize that upon bacterial lysis they persist in the phagolysosome and protect surviving bacteria. To test this, we will attempt to functionally complement mutants by exogenous addition of purified nanocompartments during macrophage infection. Purified nanocompartments will be added to infection media containing *M. tuberculosis* to promote phagocytosis of bacteria and nanocompartments in the same vesicle. To visualize the infection, bacteria will be transformed with an mCherry plasmid and nanocompartments will be fluorescently labeled with a dye that binds to exposed lysine residues. Bacterial viability will be measured over a four-day time course by plating for CFU. Additionally we will attempt to complement nanocompartment mutants *in trans* during exposure of mutant bacteria to acid and oxidative stress in broth by adding purified nanocompartments throughout a time course. Bacterial viability will again be measured by CFU enumeration.

In our study, we showed that nanocompartment mutants are attenuated during macrophage infection. However, we have not established their importance for *M. tuberculosis* virulence *in vivo.* To do this, C57BL/6 mice will be infected with wild-type and nanocompartment mutants via the aerosolization route. To test the role of nanocompartment during different stages of the immune response to infection, bacterial lung CFU will be measured at days 1 (initial infection), 10 (innate immune response), 14 (onset of adaptive immunity), and 28 (maximum adaptive immune response) post-infection. If nanocompartment mutants are attenuated in wild-type mice, we will infect NADPH oxidase knockout mice with nanocompartment mutants and measure their virulence. NADPH oxidase knockout mice are unable to produce ROS in response to infection. If nanocompartment mutants are attenuated in wild-type mice, we suspect their growth will be restored in mice unable to generate an oxidative stress response during infection.

4.3 Final thoughts

Large data sets generated by experiments like transposon sequencing screens provide insights that are simultaneously promising and daunting. One is presented with an abundance of information, but in poorly annotated species, like *M. tuberculosis*, it is challenging to determine how to prioritize and validate results. In the midst of my analysis of the first replicate of the Tn-seq screen, I was at a barbecue with friends and fellow graduate students. We were discussing our research, as scientists in any social gathering are wont to do. My friend, who studied the nanocompartment in *T. maritima,* mentioned *M. tuberculosis* has genes encoding a putative nanocompartment and was curious if they were a hit in my screen. The events that followed highlight the remarkable feature of large screen data sets: when they are approached with the right question, they yield answers that can inspire hypothesis-driven research. The nanocompartment shell, Cfp29, was attenuated in one of the macrophage conditions, and the rest is history outlined in Chapter 3.

References

1. Abel L, El-Baghdadi J, Bousfiha AA, Casanova J, Schurr E. Human genetics of tuberculosis: a long and winding road. Philosophical transactions of the Royal Society of London.Series B, Biological sciences;369(1645):20130428; 20130428-20130428.

2. Algood HMS, Chan J, Flynn JL. Chemokines and tuberculosis. Cytokine Growth Factor Rev. 2003 12/01;14(6):467-77.

3. Alonso S, Pethe K, Russell DG, Purdy GE. Lysosomal killing of *Mycobacterium* mediated by ubiquitin-derived peptides is enhanced by autophagy. Proc Natl Acad Sci USA. 2007 04/03;104(14):6031.

4. Baker LV, Brown TJ, Maxwell O, Gibson AL, Fang Z, Yates MD, et al. Molecular Analysis of Isoniazid-Resistant *Mycobacterium tuberculosis* Isolates from England and Wales Reveals the Phylogenetic Significance of the *ahpC* âˆ'46A Polymorphism. Antimicrob Agents Chemother. 2005 04/01;49(4):1455.

5. Barberis I, Bragazzi NL, Galluzzo L, Martini M. The history of tuberculosis: from the first historical records to the isolation of Koch's bacillus. Journal of preventive medicine and hygiene. 2017 03;58(1):E9-E12.

6. Bedard K, Krause K. The NOX Family of ROS-Generating NADPH Oxidases: Physiology and Pathophysiology. Physiol Rev. 2007 01/01; 2018/12;87(1):245-313.

7. Behr MA, Edelstein PH, Ramakrishnan L. Revisiting the timetable of tuberculosis. BMJ. 2018 British Medical Journal Publishing Group;362.

8. Bhaskar A, Chawla M, Mehta M, Parikh P, Chandra P, Bhave D, et al. Reengineering Redox Sensitive GFP to Measure Mycothiol Redox Potential of Mycobacterium tuberculosis during Infection. PLOS Pathogens. 2014 01/30;10(1):e1003902.

9. Bigi F, Gioffre A, Klepp L, de la PS, Alito A, Caimi K, et al. The knockout of the lprG-Rv1410 operon produces strong attenuation of Mycobacterium tuberculosis. Microb Infect. 2004 02/01;6(2):182-7.

10. Biswas T, Small J, Vandal O, Odaira T, Deng H, Ehrt S, et al. Structural insight into serine protease Rv3671c that Protects M. tuberculosis from oxidative and acidic stress. Structure (London, England : 1993). 2010 10/13;18(10):1353-63.

11. Bogdan C. Nitric oxide and the immune response. Nat Immunol. 2001 10/01;2:907.

12. Braverman J, Sogi KM, Benjamin D, Nomura DK, Stanley SA. HIF-1α Is an Essential Mediator of IFN-γ Dependent Immunity to *Mycobacterium tuberculosis*. J Immunol. 2016 08/15;197(4):1287.

13. Braverman J, Stanley SA. Nitric Oxide Modulates Macrophage Responses to *Mycobacterium tuberculosis* Infection through Activation of HIF-1α and Repression of NF-κB. J Immunol. 2017 09/01;199(5):1805.

14. Bustamante J, Aksu G, Vogt G, de Beaucoudrey L, Genel F, Chapgier A, et al. BCG-osis and tuberculosis in a child with chronic granulomatous disease. J Allergy Clin Immunol. 2007 07/01;120(1):32-8.

15. Cassidy-Amstutz C, Oltrogge L, Going CC, Lee A, Teng P, Quintanilla D, et al. Identification of a Minimal Peptide Tag for in Vivo and in Vitro Loading of Encapsulin. Biochemistry (N Y). 2016 06/21;55(24):3461-8.

16. Chan J, Fan XD, Hunter SW, Brennan PJ, Bloom BR. Lipoarabinomannan, a possible virulence factor involved in persistence of Mycobacterium tuberculosis within macrophages. Infect Immun. 1991 05;59(5):1755-61.

17. Chan J, Xing Y, Magliozzo RS, Bloom BR. Killing of virulent Mycobacterium tuberculosis by reactive nitrogen intermediates produced by activated murine macrophages. J Exp Med. 1992 04/01;175(4):1111.

18. Chao C, Tao L. Bacterial dye-decolorizing peroxidases: Biochemical properties and biotechnological opportunities. Physical Sciences Reviews. 2016 2018-12-08T08:55:24.986+01:00;1.

19. Chen L, Xie Q, Nathan C. Alkyl Hydroperoxide Reductase Subunit C (AhpC) Protects Bacterial and Human Cells against Reactive Nitrogen Intermediates. Mol Cell. 1998 05/01;1(6):795-805.

20. Contreras H, Joens MS, McMath LM, Le VP, Tullius MV, Kimmey JM, et al. Characterization of a Mycobacterium tuberculosis nanocompartment and its potential cargo proteins. The Journal of biological chemistry. 2014 06/27;289(26):18279-89.

21. Cooper AM, Dalton DK, Stewart TA, Griffin JP, Russell DG, Orme IM. Disseminated tuberculosis in interferon gamma gene-disrupted mice. J Exp Med. 1993 12/01;178(6):2243.

22. Cooper AM, Magram J, Ferrante J, Orme IM. Interleukin 12 (IL-12) is crucial to the development of protective immunity in mice intravenously infected with mycobacterium tuberculosis. J Exp Med. 1997 07/07;186(1):39-45.

23. Cooper AM, Segal BH, Frank AA, Holland SM, Orme IM. Transient loss of resistance to pulmonary tuberculosis in p47(phox-/-) mice. Infect Immun. 2000 03;68(3):1231-4.

24. Craney A, Hohenauer T, Xu Y, Navani NK, Li Y, Nodwell J. A synthetic luxCDABE gene cluster optimized for expression in high-GC bacteria. Nucleic Acids Res. 2007 03/01;35(6):e46-.

25. Cunningham-Bussel A, Zhang T, Nathan CF. Nitrite produced by Mycobacterium tuberculosis in human macrophages in physiologic oxygen impacts bacterial ATP consumption and gene expression. Proc Natl Acad Sci U S A. 2013 11/05;110(45):E4256-65.

26. Curry S, Brick P, Franks NP. Fatty acid binding to human serum albumin: new insights from crystallographic studies. Biochimica et Biophysica Acta (BBA) - Molecular and Cell Biology of Lipids. 1999 11/23;1441(2):131-40.

27. Dalla Costa E,R., Ribeiro MO, Silva M, Arnold LS, Rostirolla DC, Cafrune PI, et al. Correlations of mutations in katG, oxyR-ahpC and inhA genes and in vitro susceptibility in Mycobacterium tuberculosis clinical strains segregated by spoligotype families from tuberculosis prevalent countries in South America. BMC microbiology. 2009 02/19;9:39-.

28. DeJesus MA, Ambadipudi C, Baker R, Sassetti C, Ioerger TR. TRANSIT - A Software Tool for Himar1 TnSeq Analysis. PLOS Computational Biology. 2015 10/08;11(10):e1004401.

29. Drage MG, Tsai H, Pecora ND, Cheng T, Arida AR, Shukla S, et al. Mycobacterium tuberculosis lipoprotein LprG (Rv1411c) binds triacylated glycolipid agonists of Toll-like receptor 2. Nature Structural &Amp; Molecular Biology. 2010 08/08;17:1088.

30. Dubos RJ. THE EFFECT OF LIPIDS AND SERUM ALBUMIN ON BACTERIAL GROWTH. J Exp Med. 1947 01/01;85(1):9-22.

31. Ehrt S, Schnappinger D, Bekiranov S, Drenkow J, Shi S, Gingeras TR, et al. Reprogramming of the Macrophage Transcriptome in Response to Interferon-Î³ and *Mycobacterium tuberculosis*. J Exp Med. 2001 10/15;194(8):1123.

32. Flynn JL, Chan J, Triebold KJ, Dalton DK, Stewart TA, Bloom BR. An essential role for interferon gamma in resistance to Mycobacterium tuberculosis infection. J Exp Med. 1993 12/01;178(6):2249.

33. Flynn JL, Chan J. Immunology of Tuberculosis. Annu Rev Immunol. 2001 04/01; 2018/12;19(1):93-129.

34. Giessen TW, Silver PA. Widespread distribution of encapsulin nanocompartments reveals functional diversity. Nature Microbiology. 2017 03/06;2:17029.

35. Giffin MM, Raab RW, Morganstern M, Sohaskey CD. Mutational Analysis of the Respiratory Nitrate Transporter NarK2 of Mycobacterium tuberculosis. PLOS ONE. 2012 09/18;7(9):e45459.

36. Girotti AW. Lipid hydroperoxide generation, turnover, and effector action in biological systems. J Lipid Res. 1998 08/01;39(8):1529-42.

37. Gombart AF. The vitamin D-antimicrobial peptide pathway and its role in protection against infection. Future microbiology. 2009 11;4(9):1151-65.

38. Griffin JE, Gawronski JD, DeJesus MA, Ioerger TR, Akerley BJ, Sassetti CM. High-Resolution Phenotypic Profiling Defines Genes Essential for Mycobacterial Growth and Cholesterol Catabolism. PLOS Pathogens. 2011 09/29;7(9):e1002251.

39. Guo XV, Monteleone M, Klotzsche M, Kamionka A, Hillen W, Braunstein M, et al. Silencing Essential Protein Secretion in *Mycobacterium smegmatis* by Using Tetracycline Repressors. J Bacteriol. 2007 07/01;189(13):4614.

40. Harding CV, Boom WH. Regulation of antigen presentation by Mycobacterium tuberculosis: a role for Toll-like receptors. Nature reviews.Microbiology. 2010 04;8(4):296-307.

41. Havlir DV, Barnes PF. Tuberculosis in Patients with Human Immunodeficiency Virus Infection. N Engl J Med. 1999 02/04; 2018/12;340(5):367-73.

42. 39. Ibarguren M, Lopez DJ, Escriba PV. The effect of natural and synthetic fatty acids on membrane structure, microdomain organization, cellular functions and human health. Biochimica et Biophysica Acta (BBA) - Biomembranes; Membrane Structure and Function: Relevance in the Cell's Physiology, Pathology and Therapy. 2014 06/01;1838(6):1518-28.

43. Jenkins HE, Zignol M, Cohen T. Quantifying the burden and trends of isoniazid resistant tuberculosis, 1994-2009. PloS one. 2011 07/29;6(7):e22927; e22927-e22927.

44. Kaur A, Van PT, Busch CR, Robinson CK, Pan M, Pang WL, et al. Coordination of frontline defense mechanisms under severe oxidative stress. Mol Syst Biol. 2010 01/01;6(1):393.

45. Kim B, Shenoy AR, Kumar P, Bradfield CJ, MacMicking JD. IFN-inducible GTPases in host cell defense. Cell host & microbe. 2012 10/18;12(4):432-44.

46. Kim B, Shenoy AR, Kumar P, Das R, Tiwari S, MacMicking JD. A Family of IFN-γ Inducible 65-kD GTPases Protects Against Bacterial Infection. Science. 2011 05/06;332(6030):717.

47. Kramnik I, Beamer G. Mouse models of human TB pathology: roles in the analysis of necrosis and the development of host-directed therapies. Seminars in immunopathology. 2016;38(2):221-37.

48. Larsen MH, Biermann K, Jacobs , William R. Laboratory Maintenance of Mycobacterium tuberculosis. Current Protocols in Microbiology. 2017 11/01; 2018/12;6(1):10A.1.1,10A.1.8.

49. Lee PPW, Chan K, Jiang L, Chen T, Li C, Lee T, et al. Susceptibility to Mycobacterial Infections in Children With X-Linked Chronic Granulomatous Disease: A Review of 17 Patients Living in a Region Endemic For Tuberculosis. Pediatr Infect Dis J. 2008;27(3).

50. Long JE, DeJesus M, Ward D, Baker RE, Ioerger T, Sassetti CM. Identifying Essential Genes in Mycobacterium tuberculosis by Global Phenotypic Profiling. In: Lu LJ, editor. Gene Essentiality: Methods and Protocols. New York, NY: Springer New York; 2015. p. 79-95.

51. Luthra A, Mahmood A, Arora A, Ramachandran R. Characterization of Rv3868, an Essential Hypothetical Protein of the ESX-1 Secretion System in Mycobacterium tuberculosis. J Biol Chem. 2008 12/26;283(52):36532-41.

52. MacMicking JD, North RJ, LaCourse R, Mudgett JS, Shah SK, Nathan CF. Identification of nitric oxide synthase as a protective locus against tuberculosis. Proc Natl Acad Sci USA. 1997 05/13;94(10):5243.

53. MacMicking JD, Taylor GA, McKinney JD. Immune Control of Tuberculosis by IFN-γ Inducible LRG-47. Science. 2003 10/24;302(5645):654.

54. Malm S, Tiffert Y, Micklinghoff J, Schultze S, Joost I, Weber I, et al. The roles of the nitrate reductase NarGHJI, the nitrite reductase NirBD and the response regulator GlnR in nitrate assimilation of Mycobacterium tuberculosis. Microbiology. 2009;155(4):1332-9.

55. McHugh CA, Fontana J, Nemecek D, Cheng N, Aksyuk AA, Heymann JB, et al. A virus capsid-like nanocompartment that stores iron and protects bacteria from oxidative stress. EMBO J. 2014 09/01;33(17):1896.

56. Menzies NA, Wolf E, Connors D, Bellerose M, Sbarra AN, Cohen T, et al. Progression from latent infection to active disease in dynamic tuberculosis transmission models: a systematic review of the validity of modelling assumptions. The Lancet Infectious Diseases. 2018 08/01; 2018/12;18(8):e228-38.

57. Mestas J, Hughes CCW. Of Mice and Not Men: Differences between Mouse and Human Immunology. J Immunol. 2004 03/01;172(5):2731.

58. Mishra BB, Rathinam VAK, Martens GW, Martinot AJ, Kornfeld H, Fitzgerald KA, et al. Nitric oxide controls the immunopathology of tuberculosis by inhibiting NLRP3 inflammasome-dependent processing of IL-1β. Nat Immunol. 2013 01;14(1):52-60.

59. Mishra S, Imlay J. Why do bacteria use so many enzymes to scavenge hydrogen peroxide? Arch Biochem Biophys. 2012 09/15;525(2):145-60.

60. Modlin RL, Bloom BR. TB or Not TB: That Is No Longer the Question. Science Translational Medicine. 2013 11/27;5(213):213sr6.

61. Nathan C. Neutrophils and immunity: challenges and opportunities. Nature Reviews Immunology. 2006 02/17;6:173.

62. Nathan C, Shiloh MU. Reactive oxygen and nitrogen intermediates in the relationship between mammalian hosts and microbial pathogens. Proc Natl Acad Sci USA. 2000 08/01;97(16):8841.

63. Newton GL, Buchmeier N, Fahey RC. Biosynthesis and Functions of Mycothiol, the Unique Protective Thiol of *Actinobacteria*. Microbiol Mol Biol Rev. 2008 09/01;72(3):471.

64. Nichols RJ, Cassidy-Amstutz C, Chaijarasphong T, Savage DF. Encapsulins: molecular biology of the shell. Crit Rev Biochem Mol Biol. 2017 09/03;52(5):583-94.

65. Ortalo-Magne A, Lemassu A, Laneelle M.A., Bardou F, Silve G, Gounon P, et al. Identification of the surface-exposed lipids on the cell envelopes of Mycobacterium tuberculosis and other mycobacterial species. J Bacteriol. 1996 01;178(2):456-61.

66. Pradhan G, Shrivastva R, Mukhopadhyay S. Mycobacterial PknG Targets the Rab7l1 Signaling Pathway To Inhibit Phagosome-Lysosome Fusion. J Immunol. 2018 09/01;201(5):1421.

67. Qu H, Fisher-Hoch S, McCormick JB. Molecular immunity to mycobacteria: knowledge from the mutation and phenotype spectrum analysis of Mendelian susceptibility to mycobacterial diseases. International journal of infectious diseases : IJID : official publication of the International Society for Infectious Diseases. 2011 05;15(5):e305-13.

68. Rahmanpour R, Bugg TDH. Assembly in vitro of Rhodococcus jostii RHA1 encapsulin and peroxidase DypB to form a nanocompartment. FEBS J. 2013 05/01; 2018/12;280(9):2097-104.

69. Rengarajan J, Bloom BR, Rubin EJ. Genome-wide requirements for *Mycobacterium tuberculosis* adaptation and survival in macrophages. Proc Natl Acad Sci U S A. 2005 06/07;102(23):8327.

70. Rosenberg O, Dovala D, Li X, Connolly L, Bendebury A, Finer-Moore J, et al. Substrates Control Multimerization and Activation of the Multi-Domain ATPase Motor of Type VII Secretion. Cell. 2015 04/23;161(3):501-12.

71. Russell DG. Who puts the tubercle in tuberculosis? Nature Reviews Microbiology. 2006 12/11;5:39.

72. Salins S, Newton C, Widen R, Klein TW, Friedman H. Differential induction of gamma interferon in Legionella pneumophila-infected macrophages from BALB/c and A/J mice. Infect Immun. 2001 06;69(6):3605-10.

73. Sassetti CM, Rubin EJ. Genetic requirements for mycobacterial survival during infection. Proc Natl Acad Sci U S A. 2003 10/28;100(22):12989-94.

74. Schneemann M, Schoedon G. Species differences in macrophage NO production are important. Nat Immunol. 2002 02/01;3:102.

75. Segaert S. Vitamin D Regulation of Cathelicidin in the Skin: Toward a Renaissance of Vitamin D in Dermatology? J Invest Dermatol. 2008 04/01;128(4):773-5.

76. Selvaraj P. Chapter thirteen - Vitamin D, Vitamin D Receptor, and Cathelicidin in the Treatment of Tuberculosis. In: Litwack G, editor. Vitamins & Hormones. Academic Press; 2011. p. 307-25.

77. Smith CM, Proulx MK, Olive AJ, Laddy D, Mishra BB, Moss C, et al. Tuberculosis Susceptibility and Vaccine Protection Are Independently Controlled by Host Genotype. mBio. 2016 09/20;7(5):e01516-16.

78. Sugano Y, Muramatsu R, Ichiyanagi A, Sato T, Shoda M. DyP, a Unique Dye-decolorizing Peroxidase, Represents a Novel Heme Peroxidase Family: ASP171 REPLACES THE DISTAL HISTIDINE OF CLASSICAL PEROXIDASES. J Biol Chem. 2007 12/14;282(50):36652-8.

79. Sugano Y, Nakano R, Sasaki K, Shoda M. Efficient Heterologous Expression in*Aspergillus oryzae* of a Unique Dye-Decolorizing Peroxidase, DyP, of *Geotrichum candidum* Dec 1. Appl Environ Microbiol. 2000 04/01;66(4):1754.

80. Sutter M, Boehringer D, Gutmann S, Gunther S, Prangishvili D, Loessner MJ, et al. Structural basis of enzyme encapsulation into a bacterial nanocompartment. Nature Structural &Amp; Molecular Biology. 2008 08/31;15:939.

81. Timmins GS, Deretic V. Mechanisms of action of isoniazid. Mol Microbiol. 2006 12/01; 2018/12;62(5):1220-7.

82. Tiwari S, Choi H, Matsuzawa T, Pypaert M, MacMicking JD. Targeting of the GTPase Irgm1 to the phagosomal membrane via PtdIns(3,4)P(2) and PtdIns(3,4,5)P(3) promotes immunity to mycobacteria. Nat Immunol. 2009 08;10(8):907-17.

83. Uchida T, Sasaki M, Tanaka Y, Ishimori K. A Dye-Decolorizing Peroxidase from Vibrio cholerae. Biochemistry (N Y). 2015 11/03;54(43):6610-21.

84. van dV. Albumin as Fatty Acid Transporter. Drug Metabolism and Pharmacokinetics. 2009;24(4):300-7.

85. Vandal OH, Pierini LM, Schnappinger D, Nathan CF, Ehrt S. A membrane protein preserves intrabacterial pH in intraphagosomal Mycobacterium tuberculosis. Nat Med. 2008 07/20;14:849.

86. Vandal OH, Roberts JA, Odaira T, Schnappinger D, Nathan CF, Ehrt S. Acid-susceptible mutants of Mycobacterium tuberculosis share hypersusceptibility to cell wall and oxidative stress and to the host environment. J Bacteriol. 2009 01;191(2):625-31.

87. Vogt G, Nathan C. In vitro differentiation of human macrophages with enhanced antimycobacterial activity. J Clin Invest. 2011 10/03;121(10):3889-901.

88. Weinberg JB. Nitric oxide production and nitric oxide synthase type 2 expression by human mononuclear phagocytes: a review. Mol Med. 1998 09;4(9):557-91.

89. Wetmore KM, Price MN, Waters RJ, Lamson JS, He J, Hoover CA, et al. Rapid Quantification of Mutant Fitness in Diverse Bacteria by Sequencing Randomly Bar-Coded Transposons. mBio. 2015 07/01;6(3):e00306-15.

90. Wilson M, DeRisi J, Kristensen H, Imboden P, Rane S, Brown PO, et al. Exploring drug-induced alterations in gene expression in *Mycobacterium tuberculosis* by microarray hybridization. Proc Natl Acad Sci USA. 1999 10/26;96(22):12833.

91. World Health Organization. (2018). Global tuberculosis report 2018. World Health Organization. http://www.who.int/iris/handle/10665/274453. License: CC BY-NC-SA 3.0 IGO

92. Xu H, Ren D. Lysosomal Physiology. Annu Rev Physiol. 2015 02/10; 2018/12;77(1):57-80.

93. Yin H, Xu L, Porter NA. Free Radical Lipid Peroxidation: Mechanisms and Analysis. Chem Rev. 2011 10/12;111(10):5944-72.

94. Zhang YJ, Ioerger TR, Huttenhower C, Long JE, Sassetti CM, Sacchettini JC, et al. Global Assessment of Genomic Regions Required for Growth in Mycobacterium tuberculosis. PLOS Pathogens. 2012 09/27;8(9):e1002946.

95. Zhang Y, Reddy M, Ioerger T, Rothchild A, Dartois V, Schuster B, et al. Tryptophan Biosynthesis Protects Mycobacteria from CD4 T-Cell-Mediated Killing. Cell. 2013 12/05; 2018/12;155(6):1296-308.

96. Zhang Y, Scorpio A, Nikaido H, Sun Z. Role of Acid pH and Deficient Efflux of Pyrazinoic Acid in Unique Susceptibility of *Mycobacterium tuberculosis* to Pyrazinamide. J Bacteriol. 1999 04/01;181(7):2044.

97. Zhang Y, Wade MM, Scorpio A, Zhang H, Sun Z. Mode of action of pyrazinamide: disruption of Mycobacterium tuberculosis membrane transport and energetics by pyrazinoic acid. J Antimicrob Chemother. 2003 11/01;52(5):790-5.